Geochemistry, Geophysics, Geosystems

RESEARCH ARTICLE
10.1029/2020GC009446

Deciphering Co-Seismic Sedimentary Processes in the Mediterranean Sea Using Elemental, Organic Carbon, and Isotopic Data

A. Polonia[1], C. Bonetti[2], J. Bonetti[2], M. N. Çağatay[3], A. Gallerani[1], L. Gasperini[1], C. H. Nelson[4], and S. Romano[1]

[1]Institute of Marine Sciences, National Research Council (ISMAR-CNR), Bologna, Italy, [2]Federal University of Santa Catarina, Florianopolis, Brazil, [3]Department of Geological Engineering and EMCOL Research Centre, Istanbul Technical University, Istanbul, Turkey, [4]CSIC, Instituto Andaluz de Ciencias de la Tierra, Granada, Spain

Key Points:

- Analysis of elemental, organic carbon, and isotopic data from seismo-turbidites provides information on source to sink processes
- Statistical analysis of physical and geochemical variables enhances correlation of earthquake-triggered deposits
- The application of selected geochemical proxies in paleoseismological studies can be very effective in reconstructing past seismicity

Supporting Information:

Supporting Information may be found in the online version of this article.

Correspondence to:

A. Polonia,
alina.polonia@cnr.it

Citation:

Polonia, A., Bonetti, C., Bonetti, J., Çağatay, M. N., Gallerani, A., Gasperini, L., et al. (2021). Deciphering co-seismic sedimentary processes in the Mediterranean Sea using elemental, organic carbon, and isotopic data. *Geochemistry, Geophysics, Geosystems*, *22*, e2020GC009446. https://doi.org/10.1029/2020GC009446

Received 21 SEP 2020
Accepted 23 JUN 2021

Abstract Identification of catastrophic events recorded as resedimented deep marine deposits can be challenging because of multiple possible triggering mechanisms. This study investigates seismo-turbidites (STs) deposited in the Ionian Sea as a consequence of major historical earthquakes related to the Calabrian Arc subduction system. Taking advantage of the available sedimentological reconstructions, we focused our analysis on high-resolution X-ray fluorescence core scanner (XRF-CS), organic carbon and isotopic data to define geochemical signatures characterizing the ST units. The relationships between geochemical and sedimentological proxies were statistically tested using Pearson correlation and principal component analysis (PCA). Up to ~78% of the total variance in the data set can be reduced to three principal components which identified four elemental ratio groups associated to the degree of terrestrial/coastal influence in each major depositional unit (i.e., pelagic, ST sandy stacked units, homogenites, tsunamite-seiche laminites, and tsunamite backwash). The sample score results were evaluated together with organic carbon data in order to assess geochemical variability throughout the composite turbidite structure in different basins settings. The basal parts of the ST contain coarse-grained sediment stacks whose sources can be traced back and sedimentary processes (surficial sediment erosion/massive slope failures) can be defined using geochemical data. The topmost parts of the STs exhibit a mixed compositional character suggesting basin-wide processes such as seiche oscillations and tsunami wave erosion/backwashing. The application of selected XRF-CS based elemental ratios as proxies in paleoseismological studies can help reconstruct the seismic history of a continental margin.

Plain Language Summary Submarine paleoseismology is a widely applied method to reconstruct seismicity back in time in tectonically active regions. The Calabrian Arc in the Ionian Sea is a subduction system related to the convergence between Africa and Eurasia plates which produces uplifting coastal mountains, enhances discharge of sediments on the continental shelf and induces the frequent occurrence of earthquakes. Seismic shaking is often associated with submarine slope failures, tsunamis and deposition of seismo-turbidites which represent more than 90% of total sedimentation in the deep Mediterranean basins. We analyzed physical and geochemical data of sediment samples through a statistical approach to identify elemental ratio groups bringing information on the difference between the interseismic and co-seismic sedimentary processes, as well as the degree of terrestrial/coastal influence in marine sediments. The proposed statistical approach can be used for sediment characterization, in absence of other analytical data, providing fast information on sedimentary processes and ultimately on the seismic history of the continental margin.

1. Introduction

Earthquakes are known as one of the triggering mechanisms for generating turbidity currents since the classic study of Heezen and Ewing (1952). However, events other than earthquakes (i.e., sea level changes, rapid sediment loading, volcanism, gas hydrate dissociation, flash floods, storms, etc.), could potentially trigger sediment delivery from continental shelf and slope to the abyssal plains. Discriminating between different triggering mechanisms from analysis of sediment cores is a complex task, which needs a multidisciplinary approach to define age, structure, and composition of mass flow units (Sumner et al., 2013). Given

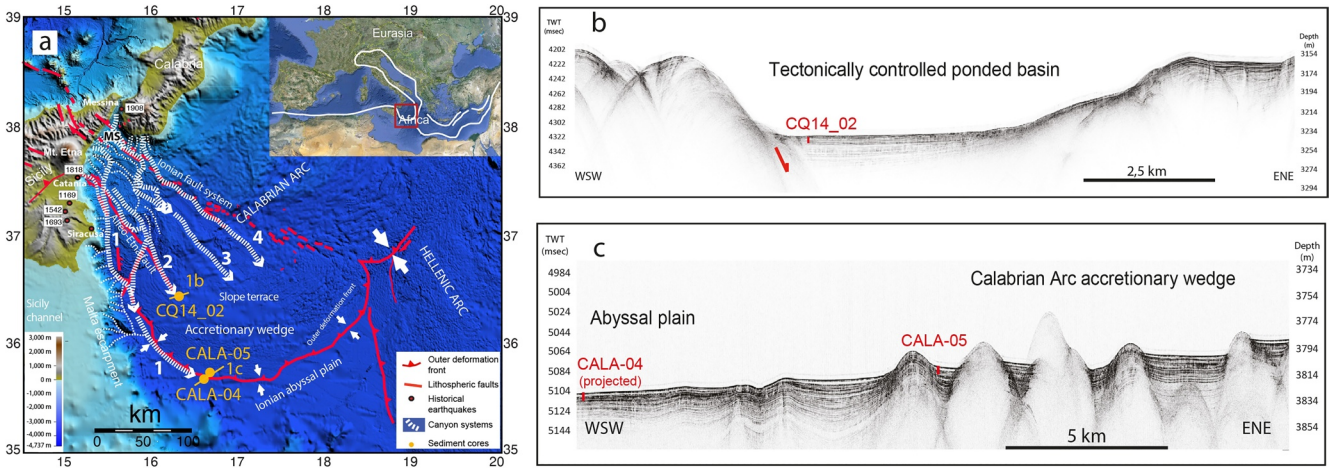

Figure 1. (a) Bathymetric map of the Ionian Sea with location of sediment cores CALA-04, CALA-05, and CQ14_02 (yellow dots) described in this study. White lines indicate major canyon systems (1–4) from the Messina Straits region down to the abyssal plain. (b) Chirp profile acquired during collection of core CQ14_02 in the slope basin directly fed by a canyon system. (c) Chirp profile acquired during collection of cores CALA-04 and -05 across the external Calabrian Arc accretionary wedge. The vertical axis on the right includes approximate depth assuming a constant sound speed of 1,500 m/s.

these limitations, the study of turbidites is a powerful tool for reconstructing the long-term earthquake history of tectonically active continental margins (Goldfinger et al., 2014 and references therein), and could potentially extend the earthquake records further back in time than historical catalogs, encompassing several seismic cycles. This approach was applied to the Calabrian Arc, one of the most seismically active region in the Mediterranean Sea, where frequent earthquakes and associated tsunamis represent the most common triggering mechanism for massive sediment remobilization in the deep basins (Kastens, 1984; Köng, Zaragosi, Schneider, Garlan, Bachèlery, San Pedro, & 2017; Köng, Zaragosi, Schneider, Garlan, Bachèlery, San Pedro, et al., 2016; Polonia, Nelson, et al., 2017; Polonia, Panieri, et al., 2013; Polonia, Romano, et al., 2015; San Pedro et al., 2017).

In turbidite studies, geochemistry is often used to reconstruct the sediment provenance, travel paths and sedimentary depositional processes (Rothwell & Croudace, 2015). However, varying factors such as climate, sea level, energy of sediment transport, redox conditions, and diagenesis in the depositional or post-depositional environment, may control the sediment geochemistry, altering the primary signatures (De Lange, 1986; Szczuciński, 2020). A detailed reconstruction of such syn- and post-depositional processes is necessary for a reliable characterization of seismically triggered turbidite deposits (hereafter called seismo-turbidites: ST). To address this issue, we focused on sediment cores that sampled STs emplaced during major historical Calabrian Arc earthquakes of 1908, 1693, and 1169 CE (Figure 1), whose stacked units were referred to different processes taking place during individual seismic events (Polonia, Nelson, et al., 2017; Polonia, Panieri, et al., 2013). Our main goal is to verify whether geochemical data of a given ST are diagnostic of co-seismic depositional processes. We used data collected from an X-ray fluorescence core scanner (XRF-CS), intensities of X-ray tomography (HU), and organic carbon (OC) data to: (a) identify geochemical proxies useful to distinguish pelagic sediments from the muddy turbidite tails; (b) characterize the geochemical composition of the STs and analyze the interplay between sedimentary processes and diagenesis; and (c) obtain information on sediment source and sedimentary processes during a ST event in different depositional settings. The results of this work in the Ionian Sea will have implications for similar studies in other tectonically active confined basins.

2. Geological Setting and Previous Work

In the Ionian Sea, one of the most seismically active regions in the Mediterranean, Africa-Eurasia plate convergence is accommodated within the subduction complex along both compressive and transtensive lithospheric faults (Polonia, Torelli, Artoni, et al., 2016; Polonia, Torelli, Gasperini, et al., 2017). Plate

convergence is associated with uplifting of coastal mountains in Calabria and northeastern Sicily, enhanced erosion, and seismic activity resulting in repetitive mass failures from the basin margins.

Five turbidite beds, deposited in the Ionian Sea during the last millennia, were studied to determine the likely triggering mechanism, provenance, and depositional processes (Polonia, Nelson, et al., 2017). Using radiocarbon and chronostratigraphic age models, it was possible to link turbidite deposition with three major tsunamigenic historical earthquakes, that is, the Mw 7.24 1908 CE Messina, Mw 7.41 1693 CE Catania, and Mw 6.6 1169 CE Eastern Sicily. Two additional turbidites were only detected in a perched slope basin directly fed by a canyon system, and appear to have been triggered by two relatively minor events, the Mw 6.23 1818 CE and Mw 6.67 1542 CE earthquakes (Figure 2).

Textural, micropaleontologic, geochemical and mineralogic analyses show that the STs have four cyclically ordered sediment units deposited during each tsunamigenic earthquake: the STa basal stacked sand unit; the STb homogenite unit; the STc tsunamite/seiche laminite unit; and the topmost STd tsunamite backwash unit (Figure 2). Such subdivision led to formulate a conceptual model for the development of tsunamigenic earthquake-triggered STs in a confined basin, where the stacked deposition of different units record the effect of sedimentary processes following seismic shaking: multiple slope failures, waning flows of the turbidity currents, water mass seiching and the slow settling from a suspension cloud created by tsunami wave erosion and sediment re-suspension (Polonia, Nelson, et al., 2017).

3. Materials and Methods

To examine STs structure and to gather information on sediment remobilization processes during large earthquakes, we used a multidisciplinary approach involving the geochemical and physical analyses of sediment cores collected in separate basins. Different parameters, such as grain size, magnetic susceptibility, CAT scan images and geochemical elemental data were acquired and integrated with stratigraphic analyses, to unravel the relationships between sediment composition, provenance, sediment structures, and ultimately the sedimentary depositional processes.

Gravity cores (CALA-04 and CALA-05) were collected during the CALAMARE cruise while the piston core (CQ14_02) was collected during the CALAQUAKE survey, carried out on board of R/V Urania in 2008 and 2014, respectively. Coring stations were selected after analysis of morphobathymetric maps and seismic reflection profiles, to sample turbidite layers at locations representative of different structural and depositional settings, and least affected by direct river inputs. Specifically, CALA-04 was collected in the open abyssal plain at 3,845 m water depth, CALA-05 in a more protected basin not far from the abyssal plain at 3,814 m water depth, and CQ14_02 in a slope terrace (3,356 m water depth) directly fed by canyons from the Messina Strait area (Figure 1).

Grain size analyses were carried out on small sample taken every centimeter interval, along the entire section for cores CALA-04 and CALA-05, and at basal coarser units for core CQ14_02, while the more homogeneous upper units in this core were sampled at 2 cm of interval. Analyses were performed using a *Beckman Coulter* LS-230 (size range 0.04–2000 μm) for cores CALA-04 and CALA-05, and a *MALVERN Mastersizer 2000* (size range from 0.02 to 2,000 μm) for core CQ14_02. Results were presented in mean diameter (MD).

Total carbon (TC) and total nitrogen (TN) were performed on bulk sediments using a *FISONS NA2000* Element Analyzer coupled to a *Finnigan Delta Plus* mass spectrometer. Total organic carbon (TOC) was determined on acidified sediment (HCl, 1.5M) to remove carbonates. TOC and TN contents are reported as weight percent (wt%) on dry weigh. C/N was calculated as molar ratio between TOC% and TN% ($14/12 \times \mathrm{TOC/TN}$). The accuracy, calculated on atropine analyses, is ±0.61% and ±0.11% for carbon and nitrogen, respectively, while precision is 2.45% and 1.92%. Determination of $CaCO_3$ was done using this relationship: $CaCO_3 = 8.33 \times (\mathrm{TC\%} - \mathrm{TOC\%})$ (Hedges & Stern, 1984; Siesser & Rogers, 1971). The mass spectrometer, fitted with a *CONFLO* interface for continuous flow measurements, was used for measurement of stable carbon isotopes in organic matter ($\delta^{13}C_{org}$), after acidification.

All core sections were scanned by a medical Core Axial Tomography scan system, under *X-ray* energy of 120 kV and pitch of 0.3. The final images (CAT scan) have a voxel size of $0.5 \times 0.5 \times 1$ mm^3 with slice thickness of 1 mm. The intensity of the transmitted *X-ray* beams is expressed as *Hounsfield Unit* (HU), which

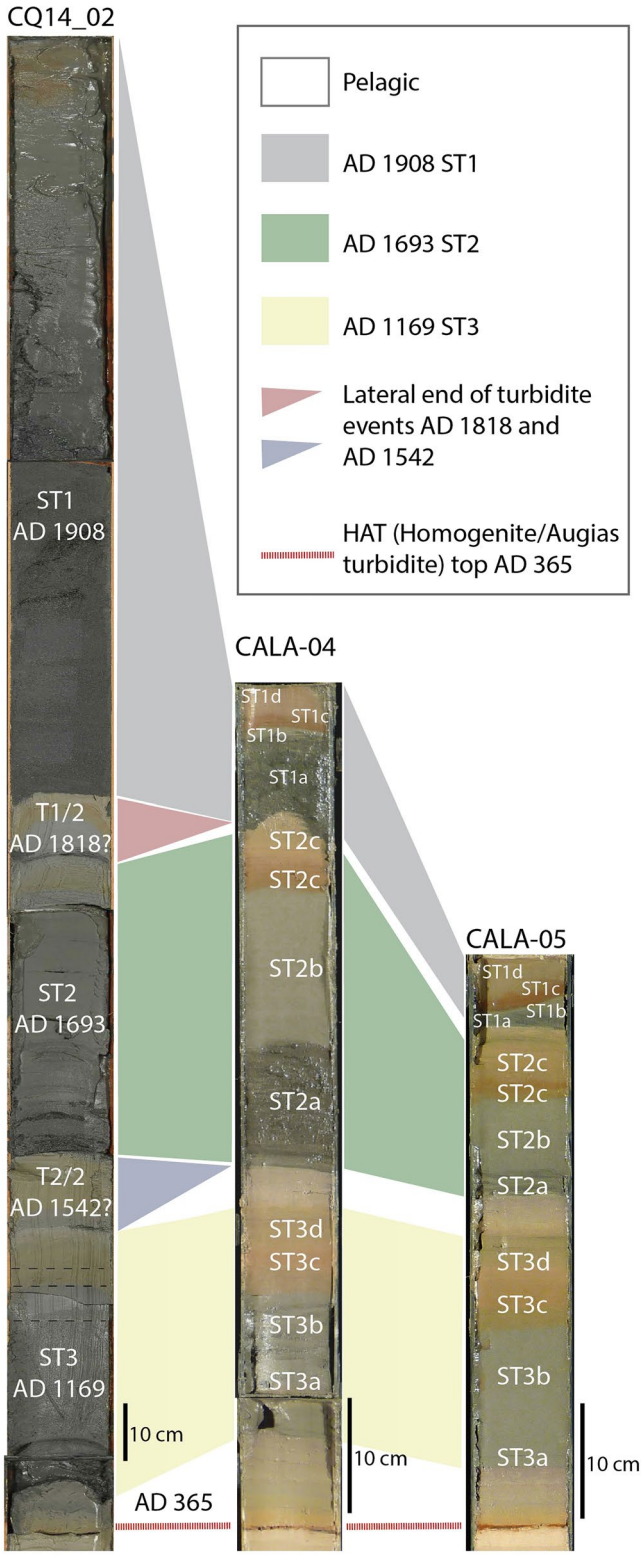

Figure 2. Correlation between turbidites in cores CALA-04, CALA-05, and CQ14_02 (Figure 1 for location). For graphical reasons the scale of core CQ14_02 is twice relative to the other cores. During the last 2,000 years more than 90% of sedimentation in these cores is represented by seismically triggered resedimented beds. The red dashed line represents the top of the Homogenite/Augias Turbidite (HAT), which was emplaced after the 365 CE earthquake and tsunami (Polonia, Bonatti, et al., 2013; Polonia, Vaiani, & De Lange, 2016). Modified from Polonia, Nelson, et al. (2017).

follow the relation: HU = $(\mu_m - \mu_w)/(\mu_w) \times 1{,}000$ where μ_w is the linear attenuation coefficient of the water, and HU depends on properties of the material (m) of X-ray absorption.

High-resolution magnetic susceptibility (MS) logs were acquired with a *Bartington*, model MS2, equipped with a 100 mm loop sensor at sampling interval of 5 mm.

Geochemical data of core CALA-05 were collected by using an *Avaatech* XRF-CS at GRC-University of Barcelona under two different settings, 10 kV (10 s measuring time) and 50 kV (30 s measuring time). CALA-04 and CQ14_02 were scanned using an *Avaatech* XRF-CS at ISMAR CNR-Bologna, under 10 kV (10 s measuring time), 30 kV (20 s measuring time) and 50 kV (30 s measuring time) settings. Measurements were performed with a step size of 1 cm along the cores. Since the main purposes of this work are to reconstruct depositional processes, to discriminate between different sediment sources and traveling paths, and to assess diagenetic processes, we selected diagnostic elemental ratios which traditionally track detrital alumino-silicates, mainly the clay minerals (e.g., Al, Si, and Rb) and heavy minerals (e.g., Zr, Fe, and Ti), carbonates (e.g., mostly biogenic; Ca and Sr), diagenesis overprint (e.g., redox-sensitive elements: Fe, Mn, and S), and porosity or interstitial water content (Cl and S) (Chester, 2000) (see Table S1 for a summary of main assumptions used in our analysis).

The Pearson product-moment correlation coefficient (Pearson's r) was used to measure the linear relationship between $CaCO_3$, OC, C/N, $\delta^{13}C_{org}$, grain size and total elemental intensities (Al, Si, S, K, Ca, Ti, Mn, Fe, Br, Rb, Sr, and Zr) and element ratios. For core CALA-04 and CQ14_02, Pb, Cu, and Zn were also considered as additional elements. The linear correlation was considered statistically significant to p-values <0.05.

A principal component analysis (PCA) based on Pearson correlation coefficients was applied to evaluate the contribution of each one of the 17 diagnostic elemental ratios to the identification of major geochemical trends in the cores, to assess the correlation between variables, and to visualize the overall relationships of the samples within the data set, including recognition of samples with anomalous geochemical behavior (outliers). Specifically, PCA is a multivariate exploratory technique that reduces a larger set of variables into a smaller set of uncorrelated "artificial" variables, called "principal components" (PC), which account for most of the variance in the original variables (Besse, 1992; Bryant & Yarnold, 1995; Davis, 1986). The dimensional reduction of the data provided by PCA is particularly useful for XRF-CS data, with a large set of elements and elemental ratios.

The contribution of each original variable to the variation of the PC (i.e., the variable loading) was used to identify the elemental ratios that contribute the most to the variation observed in the score plots, allowing to better differentiate the samples along a geochemical gradient. Elemental ratios with similar factor loadings (close together in PCA loadings plots) were considered as indicators of the same geochemical affinity. In the same way, the values of the factors scores were used to recognize samples with similar multivariate geochemical profile. By assessing the degree of overlap between sample groups within the PCA scores plots, it is possible to assess if the ST units have similar or different geochemical compositions. Since in the PCA the directions of the scores plot correspond to the directions in the loadings plot, it is possible to correlate the variables to different groups observed in the scores plot. Statistical calculations and graphics representations were processed using STATISTICA v.13 (TIBCO Software Inc, 2018), PAST v 3.25 (Hammer et al., 2001) and R (R Core Team, 2020) statistical softwares.

4. Results

XRF-CS data, combined with CAT scan, HU, core photographs, MS, MD, C/N, and $\delta^{13}C_{org}$ logs, are shown for each core in Figures 3–5. Different ST units and pelagic layers are represented by different colors.

The multiproxy analyses of sediment cores suggests that pelagic and ST units show significant differences in geochemical trends (Figures 3–5). We also note the existence of significant correlations between geochemical and sedimentological/physical properties of STs in the cores. Starting from the depositional model proposed by Polonia, Nelson, et al. (2017), we summarize the main geochemical characters among each discrete subunit forming the STs and pelagic sediments.

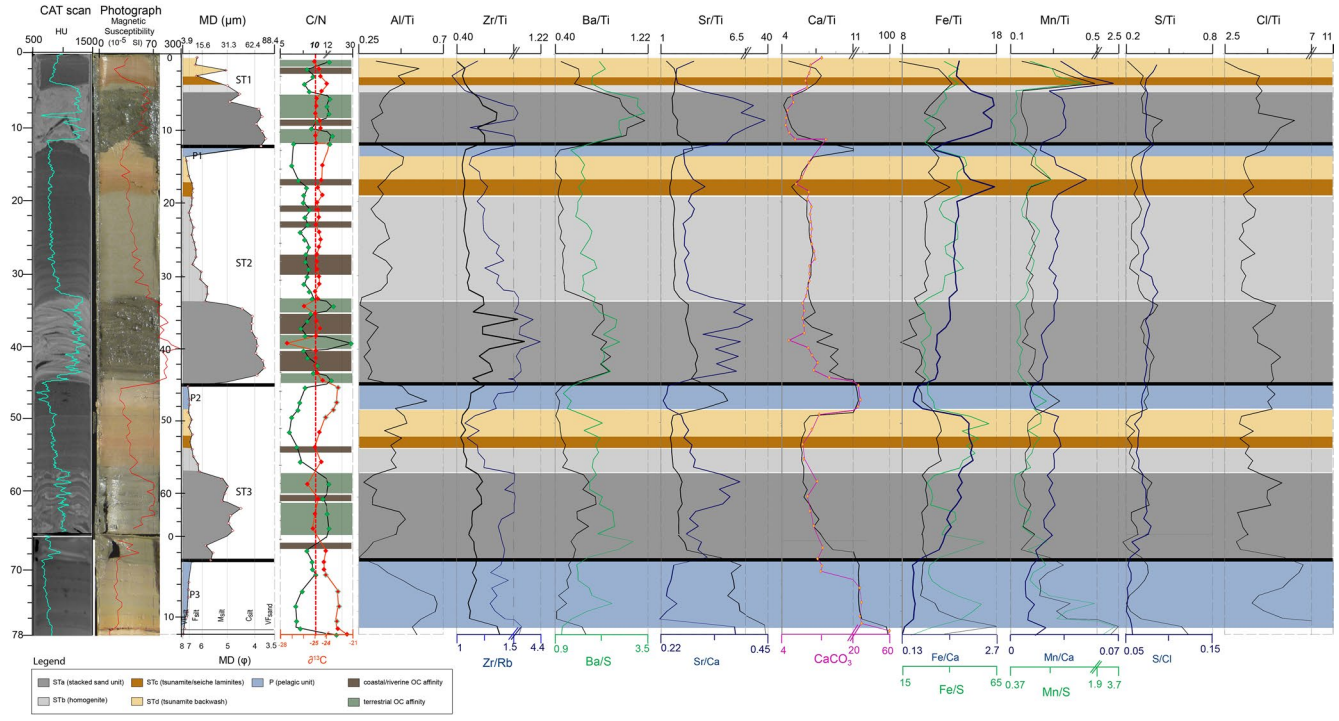

Figure 3. Log of core CALA-04. From left to right: CAT scan with HU in light blue color, photograph with high-resolution magnetic susceptibility in red, MD and subdivision in individual ST units (a–d) and pelagic units identified by different colors, C/N (green) and $\delta^{13}C$ curves (red) with organic matter mainly of marine (white layers; C/N < 10 and $\delta^{13}C_{org}$ > −25‰ VPDB) and terrestrial origins (green and brown layers; C/N > 10 and $\delta^{13}C_{org}$ < −25‰ VPDB), XRF-CS data plot along the study sample.

4.1. Physical and Geochemical Patterns of Sediment Units

Pelagic sediment units "P" (light blue in Figures 3–5) are marked by relatively high carbonate related elements (Ca/Ti and Sr/Ti) and total carbonate content ($CaCO_3$), and low values of the elements ratios indicative of detrital heavy mineral fractions. They have MD of about 7 Φ, C/N < 10, $\delta^{13}C_{org}$ > −24‰ VPDB, and peculiar features observed in CAT scan images, such as dark gray levels with abundant patches of organic matter and bioturbation (Figures 3–5).

Major ST beds (ST1, ST2, and ST3) in the different cores have similar characters. The coarse ST basal parts (STa units), with grain size varying between coarse silt to very fine sand, are marked by pulses with C/N > 10 and $\delta^{13}C_{org}$ < −25‰ VPDB (Figures 3–5). The basal units show generally a sharp increase in elements ratios characteristic of coarse detrital input (i.e., Zr/Ti, Ba/Ti, and Fe/Ca), high values of MS and HU, low Ca/Ti and carbonate content and high Sr/Ca. Within this STa units, we note distinct layers characterized by fluctuations in grain size and element ratios (Figures 3–5): increased Zr/Ti, Ba/Ti, and Sr/Ca correspond with peaks of MD, MS, HU, and C/N, and with low values of Ca/Ti and Al/Ti, the latter increasing with a decrease in the grain size. These trends are less evident in core CALA-05, where turbidite beds are thinner and variations are shown only in the HU trend with a millimetric resolution.

The overlying fining upward homogenite (STb) parts show a sharp decrease in MD, MS and HU, while C/N fluctuates slightly between 8 to 9 and $\delta^{13}C$ between −24‰ to −25‰ VPDB (light gray units in Figures 3–5). In CALA-05 ST2b, two peaks in C/N up to a ratio of 13 and $\delta^{13}C_{org}$ values as low as −26‰ VPDB are observed. In CQ14_02 ST2b, C/N is below 9, $\delta^{13}C$ is about −25‰ VPDB and this is associated with a gradual upward decrease in Zr/Ti, Ba/Ti, Sr/Ca, and Fe/Ca and a slight increase in Al/Ti. Prominent positive peaks of Ba/Ti, Sr/Ca, Fe/Ca, S/Ti and Cl/Ti are observed in middle part of CALA-05 ST3b.

The topmost units STc and STd show relatively high values of Mn, Fe, and Ba/S, moderate increments in Al/Ti and a decrease in S/Ti and Cl/Ti. The ST1c unit in core CALA-04, in particular, is characterized by relatively low values of C/N (around 8) and $\delta^{13}C$ (around −25‰ VPDB), and by an increment of Fe/Ti and

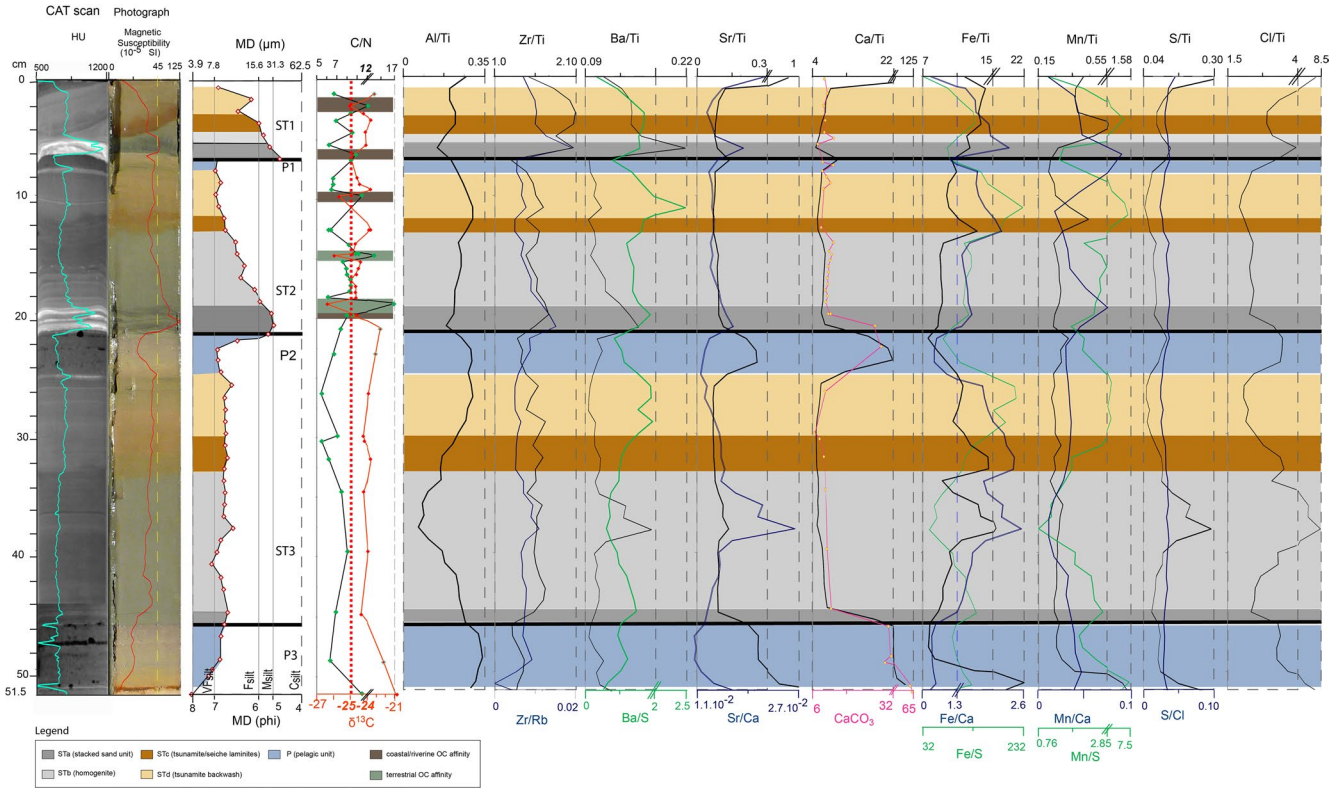

Figure 4. Log of core CALA-05. From left to wright: CAT scan with HU in light blue color, photograph with high-resolution magnetic susceptibility in red, MD and subdivision in ST (ST1, ST2, and ST3) with individual ST units (a–c) and pelagic units identified by different colors, C/N and $\delta^{13}C_{org}$ curves with organic matter mainly of marine (white layers; C/N < 10 and $\delta^{13}C_{org} > -25‰$ VPDB) and terrestrial origins (green and brown layers; C/N > 10 and $\delta^{13}C_{org} < -25‰$ VPDB), XRF-CS data plot along the study sample.

Mn/Ti. On the other hand, topmost STd1 unit in core CQ14_02 shows a further increment in C/N (ranging from 6 up to 25) and $\delta^{13}C_{org}$ (−25‰ to −24‰ VPDB), as well as by correlative peaks of MD, MS, and HU.

Cl/Ti and S/Ti trends are very similar along the STs in the studied cores, and the S/Cl ratio is almost constant throughout the cores in CALA-04 and CALA-05 (Figures 3 and 4) with increments in STa units and a progressive decrease in the uppermost units. In core CQ14_02 the ST1a unit is marked by peaks of S/Cl (pink bars in Figure 5), C/N > 12, and increases in MD and lower MS values, all associated with the presence of abundant *Posidonia oceanica*, a marine plant living in very shallow water.

ST1/2 and ST2/2 are thinner than ST1, ST2, and ST3, and are present only in core CQ14_02, which shows a more expanded record of STs. Both ST1/2 and ST2/2 turbidite beds exhibit higher values of Ca/Ti, $CaCO_3$, and Sr/Ti relative to the other STs. ST1/2 shows the same four units as in the other turbidite beds (Figure 5) all of them high in Sr/Ti and Ca/Ti; unit STc and STd has an increase in Fe and Mn. C/N is >10 in the STa, and C/N < 10 in units STb, STc, and STd.

ST2/2 which is the only turbidite bed related to a non-tsunamigenic earthquake does not show any turbidite stacks in unit STa and lacks STc and STd; moreover, transitions are more gradual compared with other turbidites (Figure 5). Concerning geochemical patterns, unit STa is high in Zr, Ba, Ca, Sr, and low in Al, while unit STb is high in Ca, Sr, and Al. C/N values are always <10 and $\delta^{13}C_{org}$ values are >−25‰ VPDB except for low values at its base.

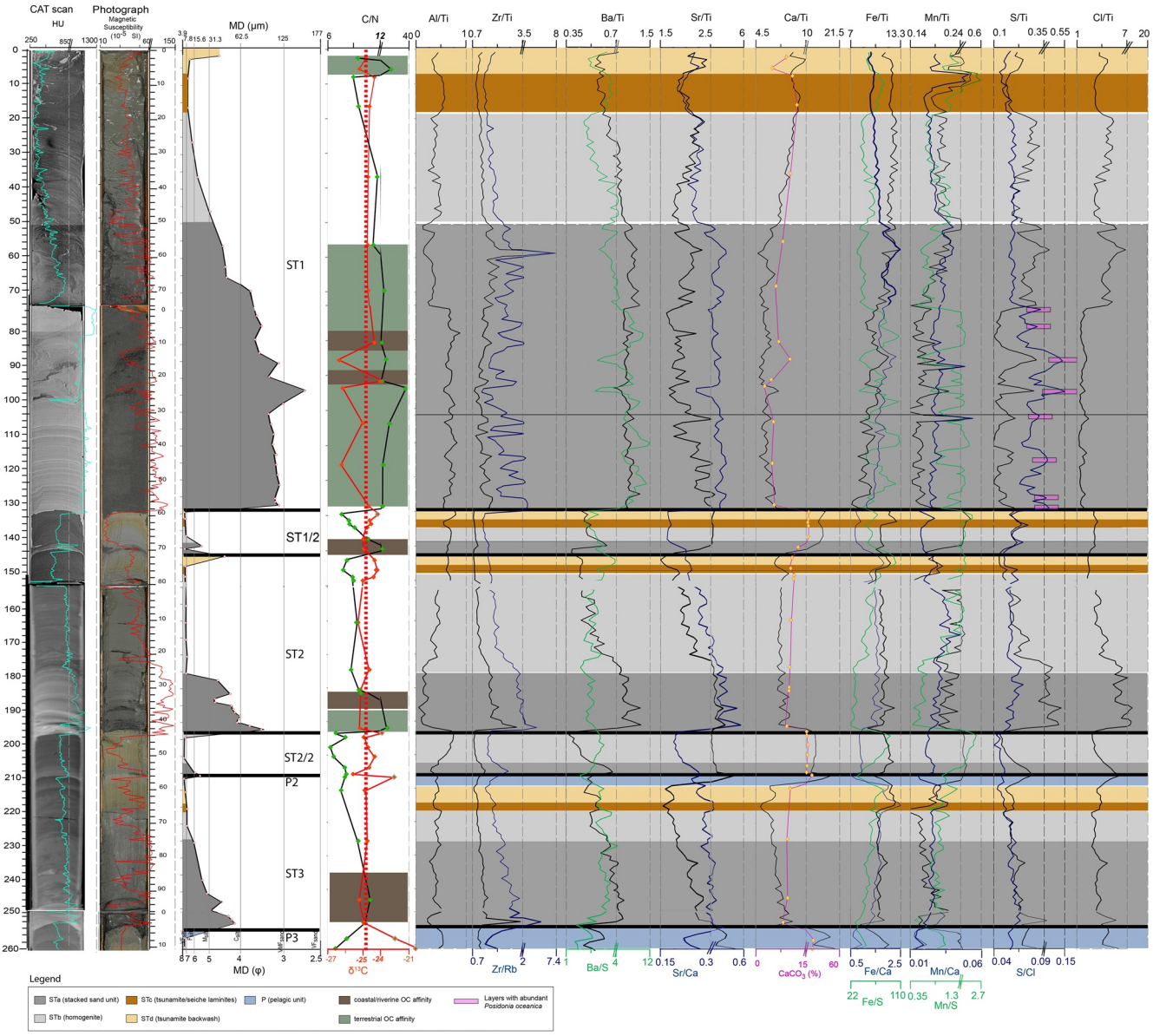

Figure 5. Log of core CQ14_02. From left to right: CAT scan with HU in light blue color, photograph with high-resolution magnetic susceptibility in red, MD with subdivision in STs (ST1, ST2, and ST3) with individual ST units (a–d) and pelagic beds shown with different colors, C/N and $\delta^{13}C_{org}$ curves with organic matter mainly of marine (white layers; C/N < 10 and $\delta^{13}C_{org}$ > −25‰ VPDB) and terrestrial origins (green and brown layers; C/N > 10 and $\delta^{13}C_{org}$ < −25‰ VPDB), XRF-CS data plot along the study sample. Pink bars on S/Cl plot indicate layers with abundant *Posidonia oceanica,* a marine plant leaving in shallow water.

4.2. Statistical Analysis

4.2.1. Relationships Among Variables

Pearson correlation analyses was performed for each core, using XRF-CS (as elemental ratios), grain size, carbonate content, TOC, C/N, and $\delta^{13}C_{org}$ data. The three matrices with the values of Pearson product-moment correlation coefficients are presented as supplementary material in Tables S2–S4. The statistically significant correlation (p-value <0.05) between sedimentological/geochemical descriptors and the main elemental ratios are represented in Table 1. Sand percentage correlates positively with C/N and negatively with carbonate content, $\delta^{13}C_{org}$ and TOC, except for core CALA-05 in which no significant correlation was found between MD and TOC. All cores also presented positive correlation between sand percentage and Zr/Rb, Zr/Ti Ba/Ti, and Sr/Ca, while clay percentage correlated positively with Ba/S and Ca/Ti. Total carbonate

Table 1
Statistically Significant Correlation (p-value <0.05) Between Sedimentological/Geochemical Descriptors and the Main Elemental Ratios

	Positive correlation			Negative correlation				Positive correlation			Negative correlation		
	CALA 4	CALA 5	CQ14-2	CALA 4	CALA 5	CQ14-2		CALA 4	CALA 5	CQ14-2	CALA 4	CALA 5	CQ14-2
MD (μm)	C/N		C/N	$CaCO_3$ TOC $\delta^{13}C$		$CaCO_3$ $\delta^{13}C$	**$CaCO_3$**	CLAY $\delta^{13}C$	$\delta^{13}C$	SILT CLAY TOC $\delta^{13}C$	MD SAND SILT	SILT	MD SAND C/N
	Zr/Rb Zr/Ti Ba/Ti Sr/Ca S/Cl	Zr/Rb Zr/Ti Ba/Ti	Zr/Rb Zr/Ti Ba/Ti Sr/Ca Fe/Ca S/Cl	Ba/S Al/Ti Fe/Ti Fe/S Mn/S	Ba/S	Ba/S Fe/Ti Fe/S Mn/S Mn/Ti Ca/Ti		Ba/S Al/Ti Fe/Ti Mn/S Mn/Ti Ca/Ti Sr/Ti Cl/Ti S/Ti	Ba/S Fe/Ti Mn/S Mn/Ti Ca/Ti Sr/Ti	Ba/S Mn/Ti Ca/Ti Sr/Ti	Fe/Ca Mn/Ca S/Cl	Fe/Ca	Zr/Rb Ba/Ti Sr/Ca Fe/Ca Mn/Ca S/Cl
SAND	C/N		C/N	$CaCO_3$ TOC $\delta^{13}C$		$CaCO_3$ TOC $\delta^{13}C$	**TOC**	SILT C/N	C/N	CLAY $CaCO_3$	MD SAND $\delta^{13}C$	$\delta^{13}C$	SAND
	Zr/Rb Zr/Ti Ba/Ti Sr/Ca S/Cl	Zr/Rb Zr/Ti Ba/Ti Sr/Ca	Zr/Rb Zr/Ti Ba/Ti Sr/Ca Fe/Ca S/Cl	Ba/S Al/Ti Fe/Ti Fe/S Mn/S		Ba/S Fe/Ti Fe/S Mn/S Mn/Ti Ca/Ti			S/Cl	Ba/S Mn/Ti Ca/Ti Sr/Ti	Zr/Rb Zr/Ti Ba/Ti Sr/Ca Cl/Ti	Fe/Ti	Zr/Rb Zr/Ti Ba/Ti Sr/Ca Fe/Ca Mn/Ca
SILT	TOC		$CaCO_3$ $\delta^{13}C$	$CaCO_3$ $\delta^{13}C$	$CaCO_3$ $\delta^{13}C$	C/N	**$\delta^{13}C$**	CLAY $CaCO_3$	$CaCO_3$	SILT CLAY $CaCO_3$	MD SAND SILT TOC C/N	SILT TOC C/N	MD SAND C/N
	Fe/Ca Fe/S Mn/Ca	Ba/Ti Mn/Ca	Ba/S Fe/Ti Fe/S Mn/S Mn/Ti Ca/Ti	Zr/Rb Zr/Ti Sr/Ca Mn/Ti Ca/Ti Sr/Ti Cl/Ti S/Ti	Ba/S Fe/Ti Ca/Ti Sr/Ti	Zr/Rb Zr/Ti Ba/Ti Sr/Ca Fe/Ca S/Cl		Ba/S Fe/Ti Mn/S Mn/Ti Ca/Ti Sr/Ti Cl/Ti S/Ti	Ba/S Fe/Ti Mn/Ti Ca/Ti Sr/Ti Cl/Ti S/Ti	Ba/S Ca/Ti Sr/Ti	Ba/Ti Fe/Ca Mn/Ca S/Cl		Ba/Ti Fe/Ca Mn/Ca S/Cl
CLAY	$CaCO_3$ $\delta_{13}C$		$CaCO_3$ TOC δ13C	C/N		C/N	**C/N**	MD SAND TOC	TOC	MD SAND	CLAY$\delta^{13}C$	$\delta^{13}C$	SILT CLAY $CaCO_3$ $\delta^{13}C$
	Ba/S Al/Ti Fe/Ti Fe/S Mn/S Mn/Ti Ca/Ti Sr/Ti	Ba/S Fe/Ti Ca/Ti Sr/Ti	Ba/S Mn/S Mn/Ti Ca/Ti	Zr/Rb Zr/Ti Ba/Ti Sr/Ca S/Cl	Zr/Ti Ba/Ti Mn/Ca	Zr/Rb Zr/Ti Ba/Ti Sr/Ca Fe/Ca Mn/Ca S/Cl		Zr/Ti Ba/Ti Sr/Ca	S/Cl	Ba/Ti S/Cl	Fe/S	Fe/Ca	Mn/S Mn/Ti Ca/Ti

content and $\delta^{13}C_{org}$ are strongly and positively correlated with each other. Carbonate-rich sediments and higher values of $\delta^{13}C_{org}$ are directly correlated with Ba/S, Mn/Ti, Ca/Ti, Sr/Ti, and inversely correlated with Fe/Ca, Mn/Ca, and S/Cl, except for the core CALA-05. The concentration of TOC is relatively high in silt (core CALA-04) and clay-sized sediments (core CQ14_02), and in cores CALA-04 and CALA-05 positively correlates with C/N and negatively with $\delta^{13}C_{org}$ (both indicators of terrigenous organic carbon). Unlike the other cores, in core CQ14_02 the TOC correlates positively with $CaCO_3$, as well as with Ba/S, Mn/Ti, Ca/Ti, and Sr/Ti, which are pelagic carbonate source and redox indicators. Negative correlations between TOC and Zr/Rb, Zr/Ti, Ba/Ti, and Sr/Ca in cores CALA-04 and CQ14_02 are related to high sandy detrital input

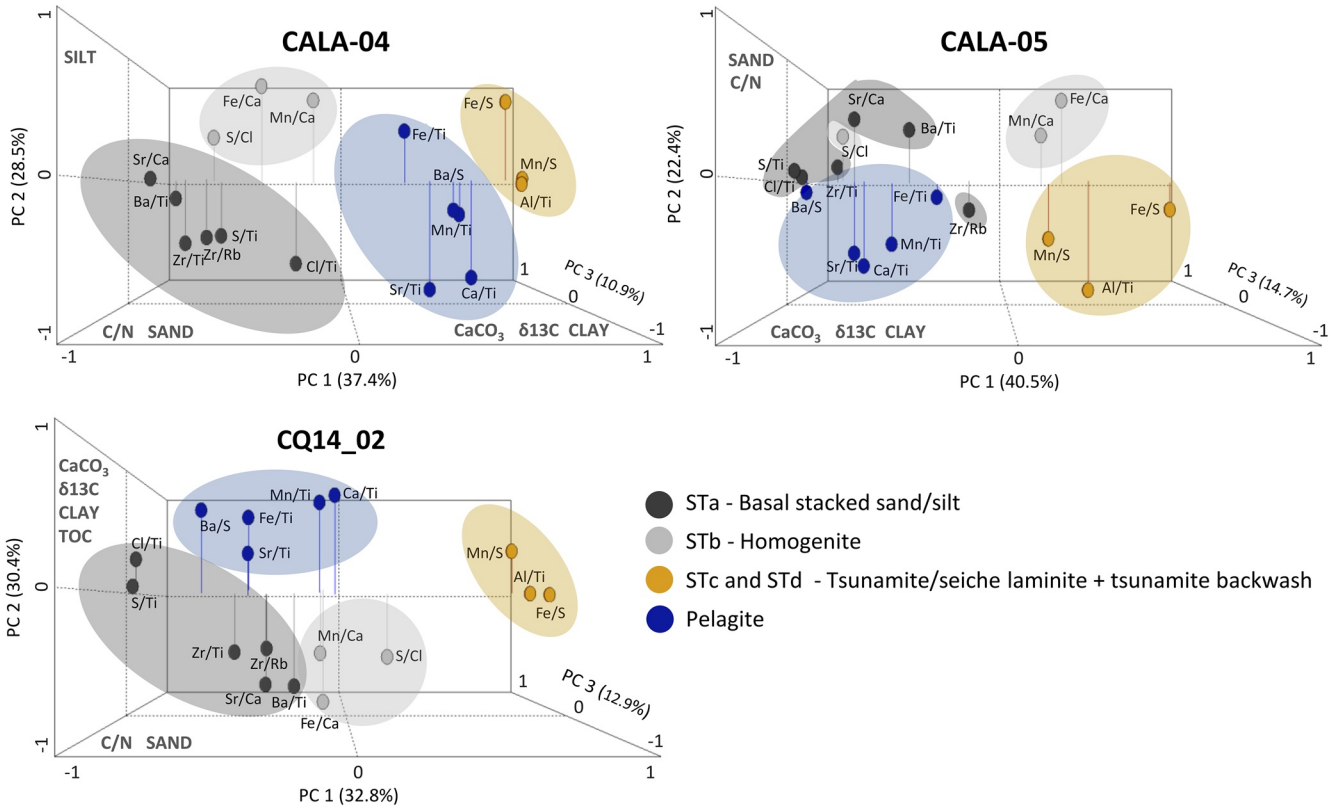

Figure 6. Correlation-scaled loading plots showing the influence of the 17 XRF-CS variables on the first components (PC 1, PC 2, and PC 3) obtained by PCA and the relationship among these variables on each core.

commonly characterized by low organic matter preservation. The input of terrigenous or coastal sediments in turbidite units, suggested by the increase of C/N and decrease of $\delta^{13}C_{org}$, is more frequently associated with increases in the Ba/Ti and S/Cl ratios.

Principal component analysis variable loadings (PCA) was applied to analyze the relationships among the set of 17 XRF-CS elemental ratios for each core, based on the Pearson correlation matrices, as summarized in Figure 6. Grain size classes, carbonate content, TOC, C/N, and $\delta^{13}C_{org}$, which were not directly included into the PCA calculations, are represented in the figure as additional variables. The first three PCs obtained for each of the cores explain over 75% of the total variance of the XRF-CS elemental ratios and allow to visualize four groups of variables. These groups have similar composition in the three cores and their distributions in the PC axes suggest that each one can be associated to previously defined depositional ST units.

4.2.2. Relationships Among Samples

The PCA - sample scores results were used to discriminate pelagic layers and the ST units, as presented in Figure 7. These results are in general agreement with the description of the units based on the individual analysis of other physical, sedimentological and geochemical descriptors plotted in Figures 3–5.

Figure 7a shows the sample score distributions for core CALA-04. The pelagite unit is well discriminated from the ST units mainly by the increase in Ca/Ti. The ST units are distributed following a regular gradient from STa (associated with higher values of Sr/Ca, among other indicators) STb, STd and at the end, to STc (higher values of Fe/S and Fe/Ca). Due to the lower values of Sr/Ti, the pelagite unit P1 is more alike to STa samples than the other pelagic layers. Each of the turbidite events described downcore (ST1, ST2, and ST3) can also be recognized along the gradient established between these PC axes. ST1a and ST2a have higher values of Sr/Ca than ST3a, which better discriminates them from the STb samples. Considering that higher values of Zr/Rb are associated with coarser (silt-fine sand) size fraction, a grain size gradient is also observed among the STs in core CALA-04, with ST2a being sandier, ST1a intermediary and ST3a less sandy.

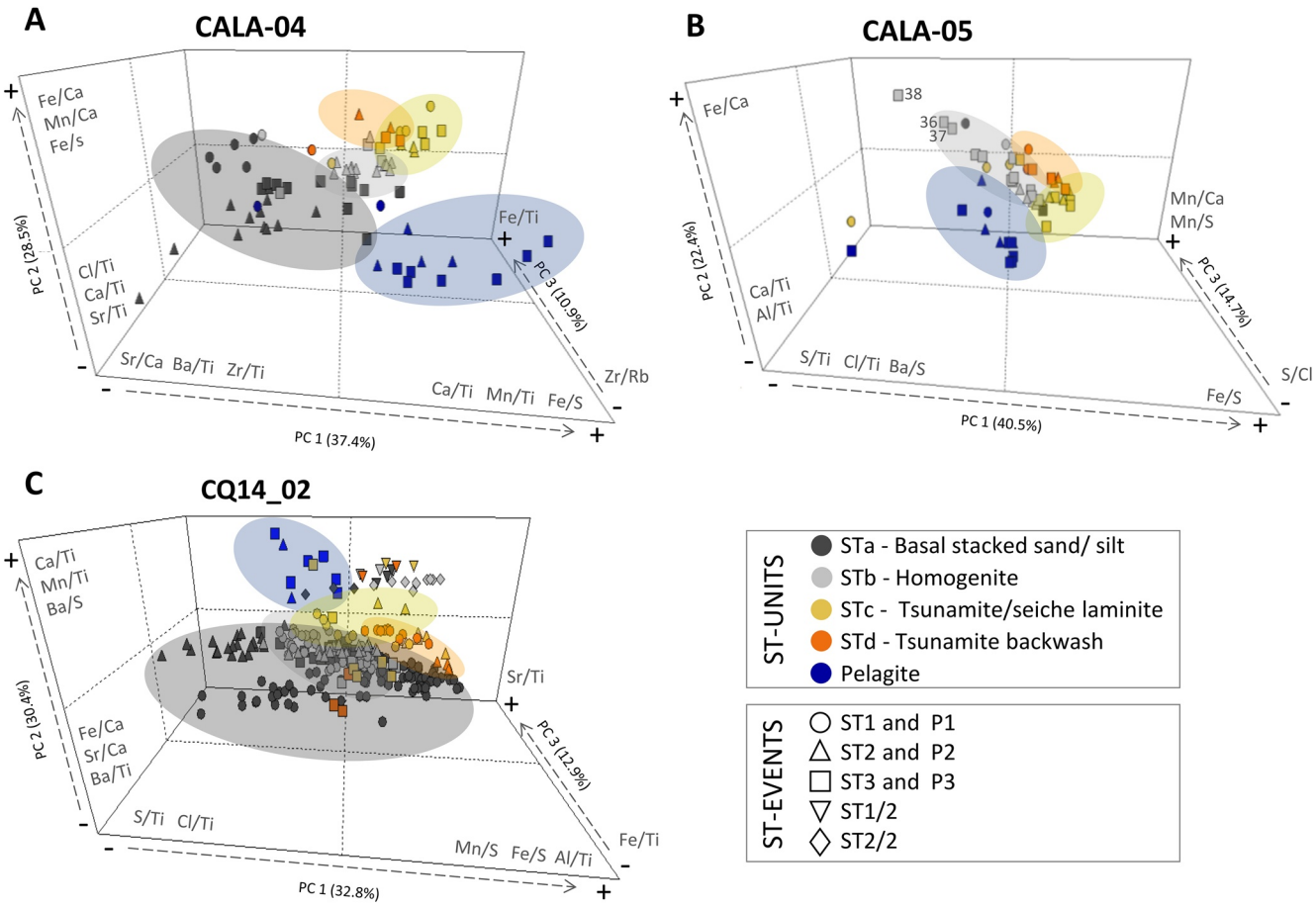

Figure 7. PCA score plots obtained from the reduction of the 17 XRF elemental ratios to three principal components (which together explain >75% of total variance) used to discriminate pelagic layers and turbidite beds and to characterize each ST unit (STa, STb, STc, STd) in the different cores (A: core CALA-04, B: core CALA-05, and C: core CQ14_02).

Figure 7b shows the sample score distributions for the CALA-05 core. The Ca/Ti gradient established through the PC2 distinguishes pelagite from the STs units, with highest values of this ratio in the pelagite unit P3. STa and STb samples are poorly differentiated from each other, which may be due to the small number of cases belonging to STa (layer with a reduced representation in this core). It is interesting to mention that samples from the depth range 36–38 cm (marked in Figure 7b) are not quite similar to those of any other ST unit. Nevertheless, the higher values of Fe/Ca, S/Ti, and lower of the Fe/S make this interval closer to the characteristics expected for STa. A gradual increase in the importance of Fe/S characterizes the STc and STd units.

Figure 7c shows the sample score distributions for the CQ14_02 core. Like the two other cores, pelagic beds are well discriminated from the ST units, reinforcing the distinct geochemical attributes of these layers. The STa unit has highest sample representativeness and also highest intra-group variability in this core. This heterogeneity is associated to an increase mainly in the values of Fe/S and Al/Ti (positive PC1 scores) in the first stage of deposition of the ST1a (samples between 75 and 133 cm depths), which makes this interval to present a geochemical behavior closer to STc and STd units. STb units are poorly discriminated in this core probably due a mixture of marine (more negative PC1 scores) and terrigenous (more positive PC1 values) origin of the sedimentary material. Most of the STc and STd samples can be distinguished from the STa and STb by the higher Fe/S values and slightly increase in the Ca/Ti. Although not as evident as the one found for CALA-04, it is possible to identify a gradient from continental to pelagic affinity moving up in the ST sequence from STa to STc. In addition to the three turbidites described for all the cores (ST1, ST2, and ST3), records of two other events found in CQ14_02 (ST1/2 and ST2/2) can also be recognized based on the results

Table 2
Summary of Seismo-Turbidites (STs) Units

Unit ID and name	Description	Depositional process
STa **Basal stacked sand/silt**	Stack of multiple graded sand/silt inputs, with different grain size and geochemical/micropaleontologic composition, some with repeated Bouma sedimentary structures.	Turbidite stacking may result from multiple earthquake-induced failures, a complex earthquake or both. Earthquake synchronously triggered turbidity currents in multiple submarine canyon and slope locations, which have different travel distances and times of arrival at the depositional site so that the sand/silt units stack one on top of another. Synchronously triggered turbidity currents that converge below multiple tributary canyon confluences
STb **Homogenite**	Multimodal clayey silt turbidite tail which gradually fines upward	Waning flows of multiple turbidity currents that are trapped in the Ionian Sea confined basin. The basin confinement traps the suspension clouds of these coeval turbidity currents that are traveling from different sources with different arrival times producing chemical variations and laminations.
STc **Tsunamite/seiche laminite**	Laminated silt unit with mm-thick white and dark orange lamina	Basin wide seiching of the confined water mass (oscillatory flow at deep water depositional sites). These forward and backwards seiche movements of the water mass can be related to the tsunami oscillator flow (Pattiaratchi and Wijeratne, 2009), to the horizontal component of earthquake surface waves (McGarr, 1965) or a combination of both. Seiching bottom currents rework sediment, which results in multiple lamina and no textural grading.
STd **Tsunamite backwash**	Topmost homogenous but graded clayey silt unit	Slow settling suspension cloud created by tsunami wave erosion or tsunami backwash of the shoreline and continental shelf. Tsunami wave may induce turbidity currents reaching to the deep sea (Arai et al. 2013). Shoreline and shelf erosion and backwash flows generate turbidity-currents, which deposit the final sediment in the Ionian Sea STs.

Note. Yellow (STa and STb): earthquake-triggered sediment units and process; Gray (STc): earthquake/tsunami triggered sediment unit and process; and Light blue (STd): tsunami backwash sediment unit and process.

of the PCA. The samples from both these events present a geochemical behavior different from the other STs, with transitional characteristics (PC scores) between STc and pelagic layers.

5. Discussion

Geochemistry is a powerful tool in reconstructing the sediment sources (detrital vs. endogenic or continental vs. marine) and transport paths of mass flow units. Applications of geochemistry in submarine paleoseismology include the analyses of inorganic tracers (Chagué-Goff et al., 2017; Goff et al., 2018; Polonia, Panieri, et al., 2013; Schwestermann et al., 2020; Yakupoğlu et al., 2019), radionuclides (Çağatay et al., 2012; McHugh, Kanamatsu, Seeber, Bopp, Cormier, & Usami, 2016; McHugh, Seeber, et al., 2020; Sakuna-Schwartz et al., 2015), organic carbon (Bao et al., 2018) and organic contaminants (e.g., PAHs

Giuliani et al., 2017; Pongpiachan & Schwarzer 2013; Tipmanee et al., 2012). The same tracers are widely used also in tsunami research onshore and in the marine environment (Chagué-Goff et al., 2017 and references therein).

In this study, we used high-resolution XRF-CS data from the Ionian Sea cores, together with organic geochemical and sedimentological proxies to characterize the individual ST units (Table 2 and Figure 8). This was performed in two steps: (a) correlation between geochemistry, sediment structure and composition and (b) application of statistical analyses to assess the relationships between geochemical patterns and sedimentary processes associated with the ST units, including the distinct sources, modes of deposition and diagenesis.

5.1. Geochemical Proxies of Ionian Sea STs Units

Pelagic sediments of the Ionian basin are represented by biogenic ooze rich in planktonic foraminifera, pteropods and shell debris (Polonia, Panieri, et al., 2013; San Pedro et al., 2017). These sediments are interbedded with turbidite beds which represent up to 90% of sedimentary succession deposited during the last 2 ka (Polonia, Panieri, et al., 2013). Our data show that the pelagic units (blue layers in Figures 3–5) are univocally identified in the studied cores by correlative peaks of Ca/Ti, Sr/Ti, and $CaCO_3$, $\delta^{13}C_{org} < -24‰$ VPDB, and low HU. On the other hand, the STs are commonly relatively enriched in detrital siliciclastic material eroded from Sicily and Calabria (Polonia, Panieri, et al., 2013). However, the STs structure and composition may vary in the different cores mainly because of different depositional settings (proximity to submarine canyons, location in isolated basins or open abyssal plain) as well as varying sediment sources, energy of the triggering event and transport paths.

5.1.1. Basal Stacked Sandy Unit STa

In all the studied cores, the STa basal units are characterized by stacked coarse sediment inputs interbedded with finer layers (Figures 3–5). The staked layers can be distinguished by their thickness, composition, and geochemical signature. In cores CALA-04 and CQ14_02 located in the abyssal plain and perched basin fed directly by canyon systems, the STas are thicker than those in more protected basins (core CALA-05), and contain several coarser-grained pulses, which suggest different arrival time of stacked sediments and amalgamated deposition. Direct correlations between Zr, Ba, Fe peaks, and MS, MD, and HU trends, indicate the enrichment of coarse silt to fine sand size detrital siliciclastic material, whose composition can be traced back to the metamorphic

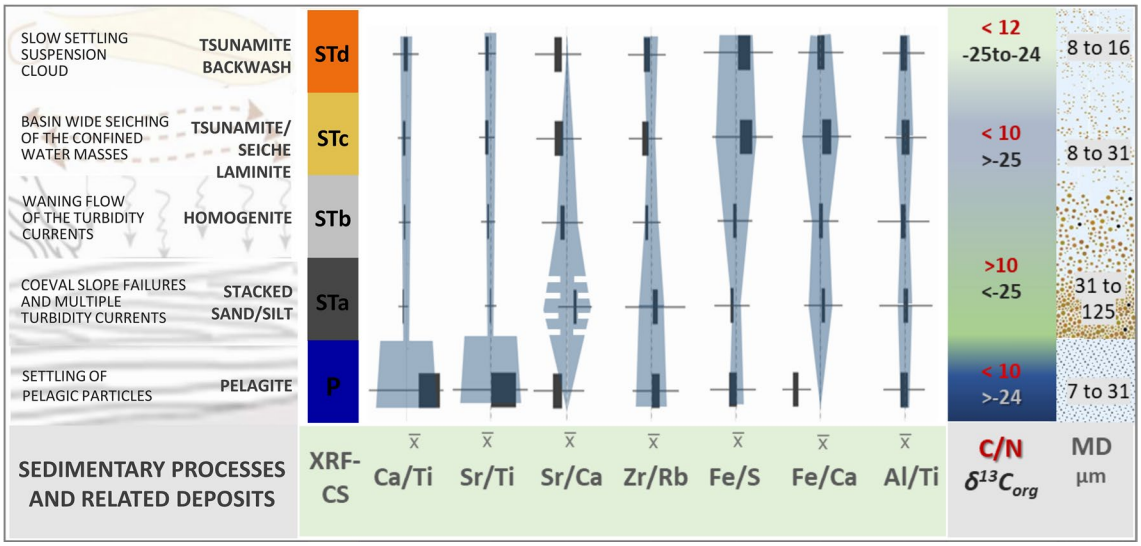

Figure 8. Schematic diagram of the variability of selected XRF-CS elemental ratios through the depositional units and their relationship with other geochemical descriptors (C/N, $\delta^{13}C_{org}$, and MD: mean diameter). The *x*-axis expresses the ratios transformed in the *z* values. The X^- represent elemental ratio means calculated from the distribution of all values throughout the three cores (all units together). The boxes indicate the confidence interval for the mean and the whiskers the mean ±2 standard deviations calculated for each depositional unit."

basement of Calabria and to the volcanoclastic material from Mt. Etna. Such coarser sediment inputs alternate with layers represented by lower values of MS, MD, and HU showing higher content of Ca/Ti, $CaCO_3$, and Sr/Ca typical of a source region rich in carbonate rocks such as the Malta escarpment and/or the shallow Sicily channel (Figure 1).

The coarse basal STas in all cores are low in Al/Ti relative to the other sub-units, except in ST1a in core CQ14_02 and middle part of ST3a in core CALA-04 (Figures 3 and 5). In core CQ14_02, the unit ST1a has a coarser grain size than the equivalent units in the other cores. The opposite trends of carbonate content and Sr/Ti in this core suggests association of Al in coarse aluminosilicate minerals, mainly plagioclase (e.g., Sun et al., 2017). The upper part of ST3a in core CALA-04 consists of coarse silt-size material, characterized by high Sr/Ca and low Al/Ti, suggesting relative enrichment in biogenic carbonate, which is most likely to be the Sr-rich aragonitic pteropod shells (Gaetani and Cohen, 2006; Keul et al., 2017). High Cl/Ti in this subunit is related to the high porosity.

Variations of major elements from ST1/2 and ST2/2 of core CQ14_02 (Figure 5) do not correlate with grain size changes at the base of the STs which appears to be related to the absence of thick coarse pulses during these events. The high levels of Ca, Sr, and $CaCO_3$ are rather constant throughout these STs, and similar to those of the pelagic units, suggesting remobilization of surficial slope pelagic sediment by earthquake shaking (e.g., Kioka et al. 2019; McHugh, Kanamatsu, Seeber, Bopp, Cormier, & Usami, 2016; McHugh, Seeber, et al., 2020) or seismic shaking affecting only a limited area with a carbonate lithology. This agrees with the reconstruction of the triggering events related to the 1818 CE Catania (ST1/2) and 1542 CE Siracusa (ST2/2) earthquakes whose epicenters are relatively close to the coring site and whose magnitudes are relatively low (Mw 6.23 and Mw 6.77, respectively) (Polonia, Nelson, et al., 2017).

In core CALA-05, collected in a confined basin setting, only relatively thin and fine STa beds were recorded (Figures 1 and 4). Here, geochemical data do not show any pulse, but only increasing of Zr, Ba, and Fe at the base of the units immediately above the undisturbed pelagic layer. However, the pulses are evident in the very high-resolution HU record, sensitive to the mm-scale laminations (white-gray bands on the CAT images in Figure 4). This implies that the stacked units forming the coarse base of the STs, although thinner than elsewhere, are recorded in the perched, isolated basin also.

5.1.2. Homogenite STb Unit

A sharp decrease in Zr and Ba mark the base of the STb units, which are also characterized by a fining upward trend (Figures 3–5). Gradual upward decrease in Zr/Ti, Zr/Rb, and Ba/Ti, and increase in Al/Ti support the fining upward trend and larger amount of clay minerals (mainly illite). The relative trends of Ca/Ti, Sr/Ti, Sr/Ca, and $CaCO_3$ depend on the relative amount of detrital siliciclastic and biogenic carbonate material in STb units. In case of high proportion of remobilized surficial biogenic material, Sr/Ti and Ca/Ti show similar upward decreasing or increasing trends with high Sr/Ca (e.g., ST1b in cores CALA-04 and CQ14_02), whereas if siliciclastic and volcaniclastic detrital material containing plagioclase predominates, Sr and Ca show opposite trends, and the carbonate content is relatively low (e.g., ST2b in core CQ14_02 and CALA-05). The high positive excursions of Sr/Ca and Ba/Ti, and of low Al/Ti in the middle of in ST3b in core CALA-05 strongly suggest input enriched in aragonitic pteropod shells, which are relatively abundant is shallow water (shelf) sediments. Similar enrichments of Fe/Ti and S/Ti in the same zone are indicative of the subsurface development of a diagenetic front in the pteropod-rich porous layer (shown by high Cl/Ti) (Figure 4). Relatively thick pelagic unit P2 overlying the ST3 show that sufficient time was available for the diagenetic process to take place below the seafloor.

In all cores, the unit STb also exhibits a decrease of C/N (always <10) and an increase of $\delta^{13}C_{org}$ (>−25), which suggests a sedimentary organic matter of marine provenance (Figures 3–5). With some rare exceptions (e.g., ST3b in core CALA-05) geochemical elemental profiles indicate that differential settling is the dominant driving process in this unit (Figures 3–5). This agrees with a previous interpretation that the "homogenite" sediment results from remobilization of sediment by multiple turbidity currents, which deposit first the STa basal sand-coarse silt stacks and then the STb homogenite mud from the waning turbidity currents (Polonia, Nelson, et al., 2017). Similar homogenite ST deposits have been described in different settings (Beck et al., 2007; Chapron et al., 1999; Van Daele et al. 2014). The macroscopic view of this type of sediment units is homogeneous (Kastens & Cita, 1981; Stanley, 1981), but detailed analysis show that

it is graded and has laminations in CT scans which is typical for homogenite/unifite deposits (Tripsanas et al., 2004). The homogenites suspension clouds, in fact, are traveling from different sources with different arrival times providing chemical variations and laminations.

5.1.3. Tsunamite/Seiche Laminite and Tsunamite Backwash Units (STc and STd)

The STc and STd units in the studied Ionian Sea cores are commonly characterized by depletion in Cl, likely related to a general decrease in porosity, and enrichment in Fe and Mn associated with reddish color changes (Figures 3–5). The same geochemical and color changes in turbidites were previously described as typical of the turbidite cap in other regions (Chaillou et al., 2007; Jarvis et al., 1998; McHugh, Kanamatsu, Seeber, Bopp, Cormier, & Usami, 2016; Thomson, Jarvis, et al., 1998; Van Os et al., 1993). The color change was explained by a general paleo-oxidation sedimentary model for turbidites rich in organic carbon (>0.5% OC) where the consumption of oxygen is driven by the oxidation of organic matter with a subsequent production of CO_2 (Buckley & Cranston 1988, Thomson, Jarvis, et al., 1998; Wilson et al. 1985). Dissolved Fe^{2+} and Mn^{2+} in the reduced sediments diffuse upwards until they meet the downward diffusing oxygen, where they are oxidized and precipitated as oxyhydroxides (Rothwell & Croudace 2015, and reference therein). In the general paleo-oxidation model S enrichment is expected below the oxidation front (Thomson, Higgs, Croudace, et al., 1993), while above the redox front a peak of Mn/Ca should be present and correlated with a decreasing pattern of Mn/Ti (Boyle 1983; Thomson, Higgs, Jarvis, et al., 1986; Thomson, Jarvis, et al., 1998 and references therein). Comparison between the upper part of the Ionian Sea STs and the oxidation model suggests that STc and STd units are related to processes other than oxidation: (a) STc show mm-sized white and red laminae, different from those of classical redox model where no lamination is described (Figures 3–5); (b) the OC and $CaCO_3$ decrease only slightly (in a range of 0.1%–0.2%, and 2%–3%, respectively) much less than that predicted by the oxidation model (Thomson, Higgs, Croudace, et al., 1993); (c) S/Cl, has a constant trend throughout the ST units (Figures 3–5), implying the absence of an anoxic zone and a consequent negligible effect of secondary diagenetic processes throughout the turbidite beds; (d) Mn/Ca shows a pattern comparable to that of Mn/Ti, except in core CALA-05, in which there is a contrasting pattern (Figure 4); and (e) Al and Ca increase in the uppermost unit STd, characterized by a coarser sediment input in the final stages of deposition (Figures 3–5).

To determine whether Fe and Mn variations in STc and STd could be related to diagenetic or different sedimentary processes, we can also consider the Fe/Ca, Al/Ti, and Sr/Ca, good tracers for sediment input from shelf and upper slope areas as shown in the basal units. In cores CALA-04 (ST1 and ST2) and CQ14_02 (ST2 and ST3) an increase in Fe/Ca and Mn/Ca in the basal part of units STd is commonly accompanied by increase in Sr/Ca and Al/Ti, Ba/S, Sr/Ca, Fe/S in the upper part of unit STd (Figures 3–5). This suggests that the Fe and Mn enrichments in STd unit are likely due to detrital input rather than diagenesis. Such detrital input is possibly related to the tsunamigenic nature of major earthquakes in this area, with the tsunami backwash currents providing terrestrial sediments in suspension and leaving a fine tsunamite backwash on top of the ST deposit (Table 2 and Figure 8). ST2 in core CALA-04, triggered by the 1693 CE earthquake/tsunami, shows a Fe peak in unit STc and a Mn peak near the base of unit STd (Figure 3). These Fe and Mn peaks are related to digenetic enrichment in a redox front. Since diagenetic Mn and Fe-enrichment takes time and need a very low sedimentation rate, we speculate that settling of the tsunamite backwash (unit STd) from water column took a considerably long time (some months). This is in agreement with a depositional model where at the end of the turbidite depositional process very fine grained, predominantly detrital sediments in low concentration does not favor flocculation and rapid deposition (Lavallee et al., 2019). This is further supported by the observation that even nearly two months after the catastrophic Haiti earthquake, a 600-m-thick plume of sediment was still suspended in the water column from 1,100 m down to the seabed (McHugh, Kanamatsu, Seeber, Bopp, Cormier, Usami, et al., 2011).

In our reconstruction, laminated STc units are caused by basin-wide seiching of the confined water mass whose forward and backwards movements can be related to the tsunami oscillator flow (Pattiaratchi & Wijeratne, 2009), to the horizontal component of earthquake surface waves (McGarr, 1965) or a combination of both (Polonia, Nelson, et al., 2017). For the historic 1908 CE earthquake, there is evidence of seiching in the Ionian Sea after the earthquake and related tsunami (Polonia, Nelson, et al., 2017) when mass movements are described as decreasing oscillations with a period of 12–14 min and amplitudes of 5–6 m lasting

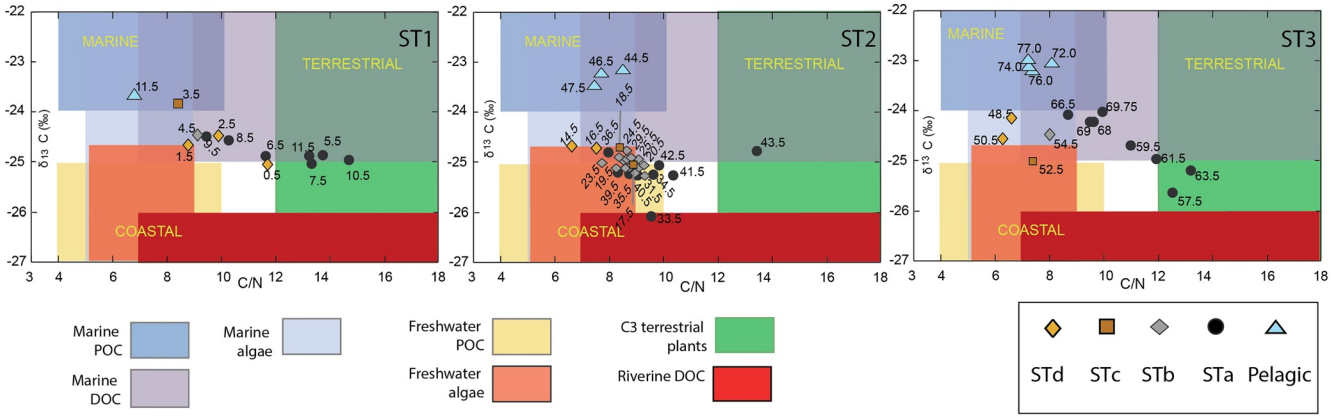

Figure 9. C/N versus $\delta^{13}C_{org}$ for the different ST units in core CALA-04. Black circles: STa; gray diamonds: STb; orange diamonds: STc; red squares: STd. The base diagram from Lamb et al. (2006). Numbers within the plots represent depth in cm of each sample within the core.

for 5 h after the main tsunami wave (Baratta, 1910). This evidence supports our interpretation that seiching oscillations in the confined Messina Straits area appear to be responsible for the deposition of STc units. Seiching bottom currents may rework sediment, resulting in multiple lamina and no textural grading. On the other hand, the coarser and shallow water input within STd unit is possibly related to tsunami triggered turbidity currents as proposed for the 2011 Tohoku-Oki earthquake (Arai et al., 2013) and to the tsunami backwash.

5.2. Sediment Unit Characterization by Multivariate Statistical Analysis of XRF-CS Data

There are only few examples in the literature regarding the investigation of earthquake-triggered sedimentary processes using PCA analysis and XRF-CS data (Chagué-Goff et al., 2017 and references therein). A multivariate statistical approach similar the one adopted in this paper was recently applied by Schwestermann et al. (2020) to characterize the main lithological units and STs in the Central Japan Trench.

In the present study, PCA analysis integrating only XRF-CS data corroborated prior results based on one-by-one interpretations of a larger set of physical and geochemical variables, allowing a statistical and less time-consuming discrimination of successive depositional units over time. Although this approach has proven to be an efficient option, the sole analysis of these ratios may lead to some challenges in the interpretation of downcore geochemical variability, considering the large changes in the elemental expression of the different turbidite units among the cores. Thereby, the application of the selected XRF-based

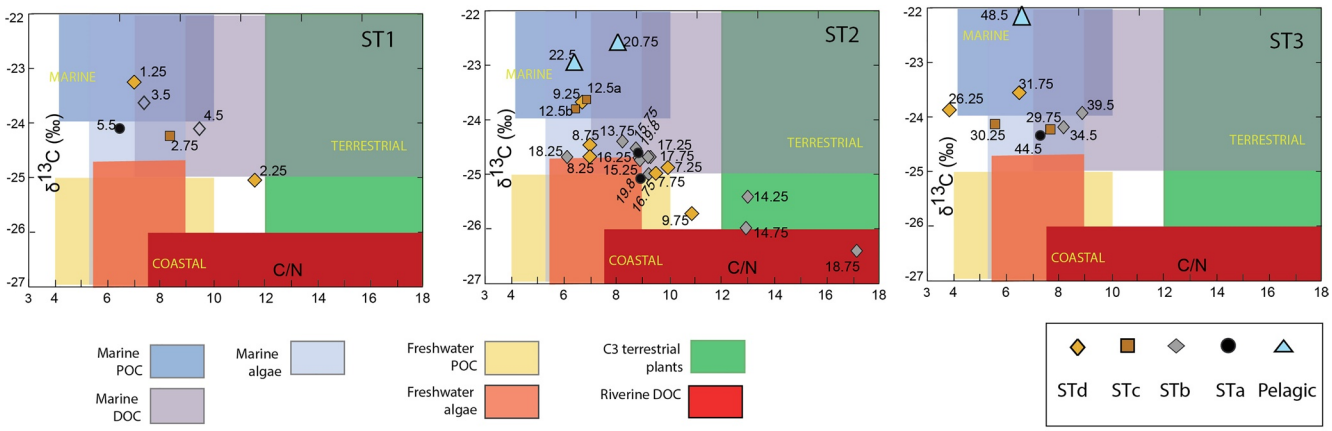

Figure 10. C/N versus $\delta^{13}C_{org}$ for the different ST units in core CALA-05. Black circles: STa; gray diamonds: STb; orange diamonds: STc; red squares: STd. The base diagram from Lamb et al. (2006). Numbers within the plots represent depth in cm of each sample within the core.

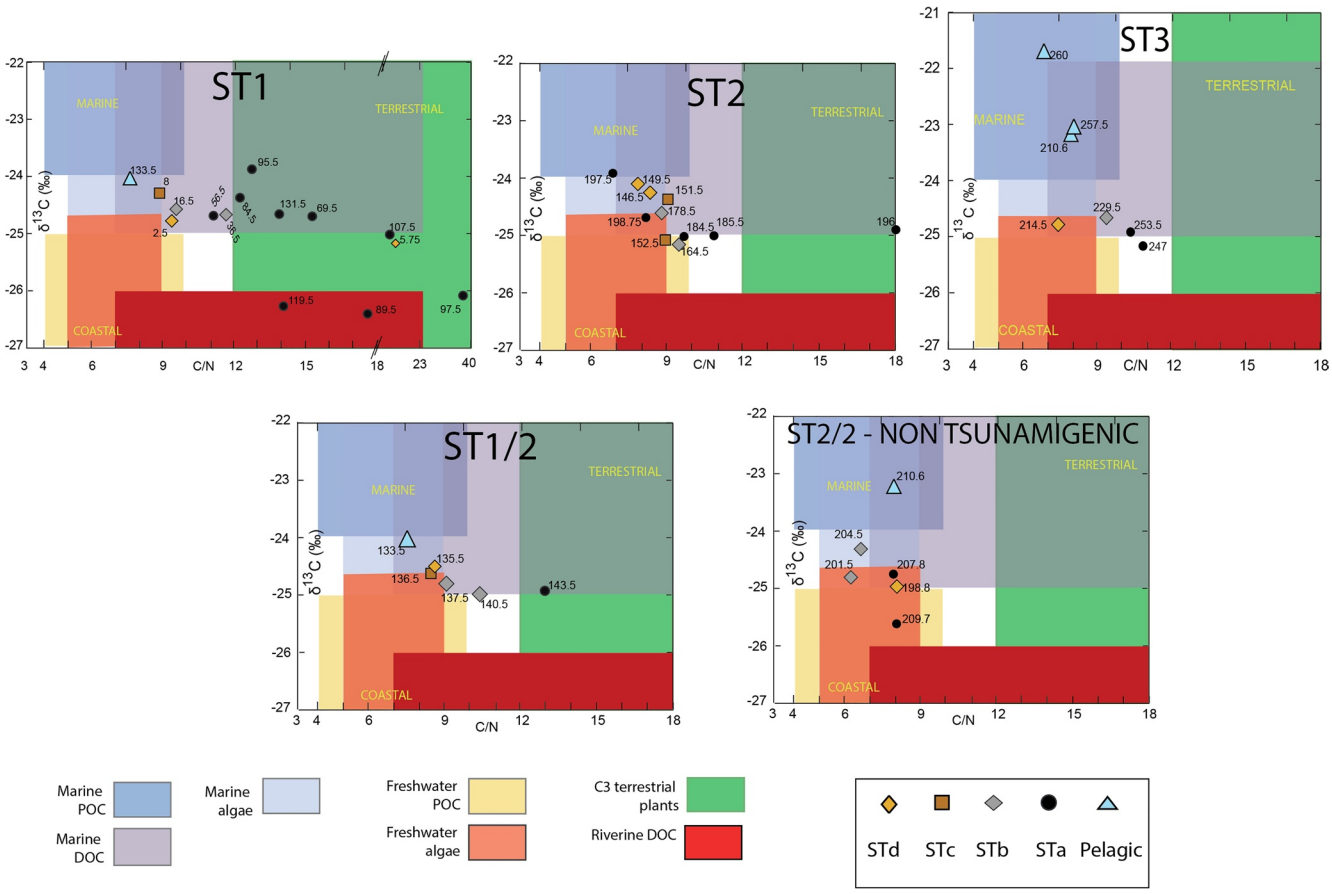

Figure 11. C/N versus $\delta^{13}C_{org}$ for the different ST units in core CQ14_02. Black circles: STa; gray diamonds: STb; orange diamonds: STc; red squares: STd. The base diagram from Lamb et al. (2006). Numbers within the plots represent depth in cm of each sample within the core.

elemental ratios as proxies in paleoseismological studies can be more effective when integrated with other lithological and geochemical descriptors (carbonate content, TOC, C/N, and $^{13}C_{org}$).

Figure 8 synthetizes the set of XRF-CS elemental ratios highlighted by the PCA analysis and organic geochemical variables suggested in this research as the ST proxies. The pelagic unit consists predominantly of biogenic constituents with lesser amounts of fine siliciclastic material and has a geochemical signature that is characterized mostly by high Sr/Ti and Ca/Ti. The unit is associated to higher contents of carbonate and clay, relatively high values of $\delta^{13}C_{org}$ (>−24‰ VPDB) and low C/N (<10). The abrupt changes from pelagic units to coarse STa basal stacked sand unit are well expressed by the peaks of Sr/Ca and Fe/Ca at the base of STa. STa is also characterized by coarser sediments (sand), and high C/N value (>10), whereas STb—homogenite graded mud is characterized by relatively low carbonate and sand contents. A decreasing gradient in the Zr/Rb and Sr/Ca is observed from basal layers toward the top in each main event deposit (ST1, ST2, and ST3), with increasing trend in Al/Ti (related to clay minerals) and Fe/S (related to fine grain size and redox conditions). STc (tsunamite/seiche laminate) and STd (tsunamite backwash) units are enriched in Fe/S. They are related to carbonate-rich, muddy sediments and have geochemical composition inversely correlated to that of the STa unit. The ST layer with the lowest proportion of terrigenous input is STc, as suggested by the geochemical variability of the different ST units in the PCA plots. The statistical descriptions of the element ratios for each individual core are present as supplementary material (S5) while the deposition processes that explain this condition are discussed in the following section.

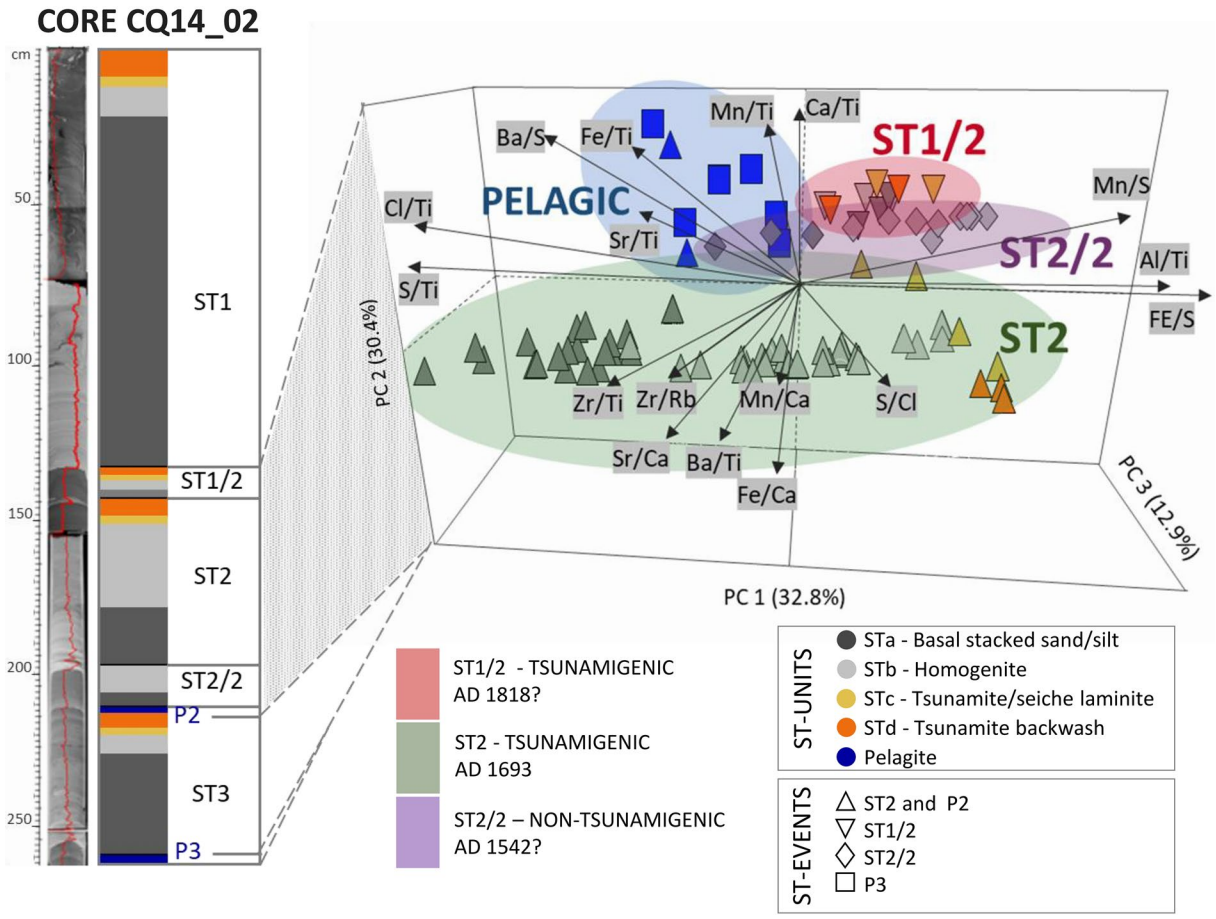

Figure 12. PCA biplot obtained from the reduction of the 17 XRF elemental ratios to three principal components used to discriminate pelagic layers and ST2, ST1/2, and ST2/2 and to characterize ST unit (STa, STb, STc, and STd) in core CQ14_02. ST1/2 and ST2/2 which are triggered by low magnitude earthquakes have geochemical characters similar to the pelagic sediments suggesting remobilization of surficial slope sediments.

5.3. Source to Sink Processes and Canyon System Activation During Seismic Shaking: Evidence From Organic Geochemistry

C/N and $\delta^{13}C_{org}$ data from the different ST units in the three cores are interpreted in order to reconstruct different sources for TOC (Figures 9–11) as proposed by Lamb et al. (2006). Samples from coarse layers in STa units show characteristic sediment pulses whose C/N and $\delta^{13}C_{org}$ values suggest riverine/coastal (brown layers in Figures 3–5) and/or terrestrial OC inputs (green layers in Figures 3–5) intercalated with beds/laminae containing organic matter of relatively high marine affinity. This result confirms that STa units are stacked (amalgamated) ST with sediments entrained by multiple turbidity currents from different slope failures which reach the coring sites at different times via separate travel paths (Figure 1). Sediments from units STa and STd are shifted toward terrestrial affinity, as corroborated by the enrichment of detrital elements (Zr, Ba, Fe/S, and Mn/S) and Sr/Ca (Figures 3–5). Units STb and STc have relatively high $\delta^{13}C_{org}$ values and low C/N < 10 implying a mainly marine provenance. The STd units are associated with relatively low $\delta^{13}C_{org}$ peaks, shifted toward coastal/freshwater and terrestrial characteristics as supported by shallow water foraminifera and coarser grain size content (Polonia, Nelson, et al., 2017).

In core CALA-04 all STs show a basal sandy unit STa with a terrestrial or riverine affinity (Figure 9). In ST1 the basal sand shows C3 terrestrial plants (green field); for ST2, only the most basal sample falls in the terrestrial field while other STa samples have a coastal/riverine affinity (orange, yellow and red fields); ST3a samples fall in the terrestrial field with the exception of the basal samples suggesting a more marine affinity, perhaps from a local slump. Because the CALA-04 deposition site is fed directly by shallow water canyon

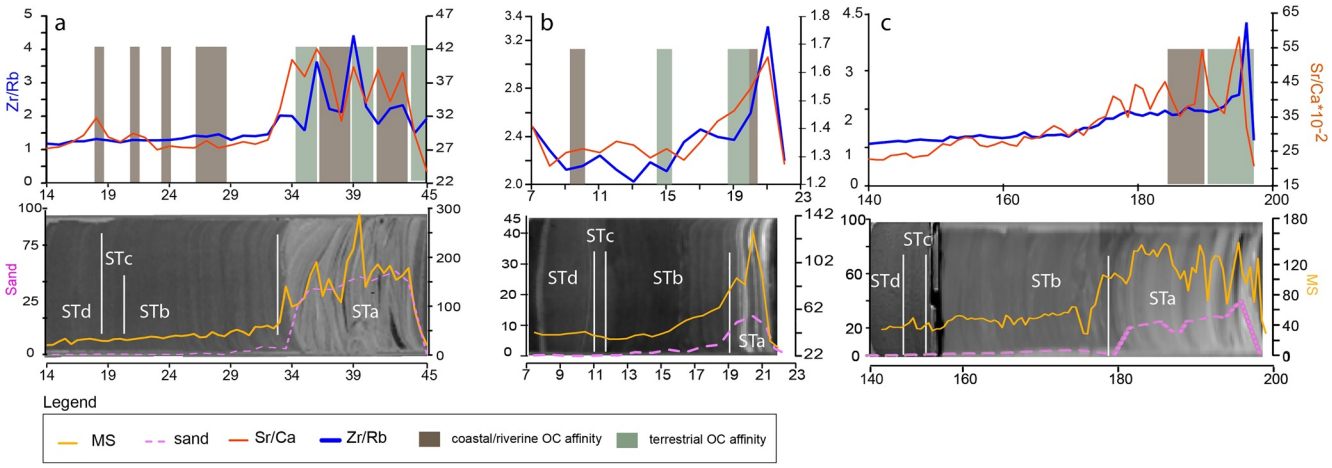

Figure 13. CAT scan, MS, grain size, Zr/Rb, and Sr/Ca for ST2 in the different cores (a) CALA-04, (b) CALA-05, and (c) CQ14_02. The brown and green bands represent riverine/coastal and terrestrial inputs respectively as deduced through the analyses of C/N and $\delta^{13}C_{org}$ (See Figures 3–5).

system 1 (Figure 1), the terrestrial/coastal composition implies that canyon 1 was activated during all major Italian earthquakes in 1908, 1693, and 1169 CE. Units STc and STd do not show a clear and uniform trend in terms of organic matter origin. However, samples from unit ST1d (orange diamonds in Figure 9) show a geochemical character similar to sub-unit ST1a with a pronounced terrestrial affinity probably from tsunami erosion and backwash sedimentation (Table 2).

In core CALA-05 (only indirectly fed by canyon system 1) the terrestrial and coastal content are less abundant (Figure 10). However, ST2 shows a more terrestrial source in this protected basin compared to the slope basin with core site CQ14_02, which is fed by canyon 2 (Figure 11). Apparently, the 1693 CE earthquake/tsunamis produced more intense effects in canyon system 1 rather than canyon system 2 where ST2 contains OC with a more pronounced marine affinity (Figure 11). ST3 in core CALA-05, on the other hand, has a composition similar to the pelagic sediments, which implies that during the 1169 CE earthquake/tsunami only limited shallow water sediment reached this more protected basin.

Core CQ14_02, in a proximal basin fed directly by canyon system 2, has a more terrestrial signal as shown by the high C/N ratio in ST1, which was emplaced during the 1908 CE Messina earthquake/tsunami (Figure 11). The terrestrial composition probably reflects the vigorous activation of canyon system 2 passing through the epicentral area of the 1908 CE earthquake, where co-seismic submarine landslides have been proposed (Billi et al., 2008; Polonia, Nelson, et al., 2017). With absence of STc and STd units, ST2/2 is the only ST that was triggered by a non-tsunamigenic earthquake. Its basal STa unit has C/N values lower than 8 and hence, fall in the marine or coastal fields (Figure 11). Seismic shaking was capable of triggering the transport of coastal material discharged on the continental shelves by river floods during interseismic periods, but apparently did not transport terrestrial C3 plants to the deep basin. This observation supports the interpretation that tsunami wave propagation and backwash did not occur during the seismic event. The PCA score plots obtained from the reduction of XRF-CS elemental ratios, show that ST1/2 and ST2/2 are geochemically more similar to pelagic sediments compared to ST2 (Figure 12). These plots indicate that the low magnitude triggering earthquake produced only remobilization of surficial slope sediment but not multiple slope failures as is the case for stronger earthquakes.

Organic geochemical data correlates well with Sr/Ca, and exhibits marked peaks and increments that corresponds with detrital matter of terrestrial affinity (Figures 3–5). This correlation suggests that Sr/Ca is a powerful tool to identify shallow water sediment input, mainly from aragonitic pteropod shells, which are remobilized from shelf and upper slope areas during the ST events.

5.4. Depositional Setting and Sedimentary Processes

The geochemical signature of the STs investigated by this study suggests that composition of the basal stacked beds in STa is directly linked to sediment sources and the proximity of canyon systems. However, STc and STd units have similar thickness and composition in all cores, which indicates that their deposition is controlled by basin-wide processes not affected by the local bathymetric setting (Figures 3–5).

We selected ST2, which is correlated with the 1693 CE $M_W = 7{,}41$ earthquake, to verify if and how geochemical data, CAT scans, MS and grain size can be used to unravel differences in event stratigraphy related to the coring site (Figure 13). The ST2a unit in the abyssal plain (core CALA-04, Figure 3) is represented by two stacked STa sub-units (40–45 and 33–40 cm), which both contain terrestrial sediment and high Sr/Ca (Figure 13). In core CALA-05 the basal part of unit STa has a marine affinity while the upper basal turbidite stack has a predominant continental source for the organic matter (Figures 13b and 10). This difference suggests that in the confined basin setting a first local slump occurred in relatively deep water before the arrival of the shallow water detrital input. In core CQ14_02, ST2a consists of two stacked coarse sub-units (179–188 and 188–198 cm) that are characterized by high values of MD, MS and sand %. C/N is always >10 and the shallow water detrital sediment of the two stacks is confirmed also by an elevated Sr/Ca profile. These observations suggest that only the basins disconnected from the canyons record a first local input of sediments with marine affinity, while basins fed directly by canyons received continental sediment that were deposited by the early stage turbidity currents. The comparison of ST structure and composition at different depositional sites may thus be used to unravel triggering mechanisms and processes. ST3 in cores CALA-04 and -05, for example, shows anomalous grain size and geochemical trends (Figures 3 and 4) relative to ST1 and ST2 and possibly a different triggering mechanism other than an earthquake (i.e., mega storm or slope failure). To resolve this issue, we analyze correlative STs in separate basins. In core CQ14_02, which is fed directly by a canyon system and where the turbidite beds are coarse and thick, ST3 has similar characteristics to ST1 and ST2 (Figure 5). This implies that different depositional sites may provide different records for the same process depending on the scale of slope failures and energy of the sedimentary process in each specific morphological setting. The marine character of ST3a in core CALA-05 may be related to the relatively low magnitude Mw 6.6 of the triggering 1169 CE earthquake, which was probably below a "peak ground velocity threshold" for generating slope failures, turbidity currents and their typical ST signatures in a confined basin not directly fed by a canyon system. This underlines the importance of site selection for paleoseismological studies, where the event stratigraphy is more expanded and continuous. This is particularly important for large earthquakes that may produce seafloor erosion and removal of previous STs or for low magnitude earthquakes, which do not produce thick sedimentary records.

6. Conclusions

We analyzed X-ray fluorescence (XRF-CS), organic carbon (OC), isotopic data and their statistical analyses to define the geochemical signature of ST, deposited during historical earthquake/tsunami events in the Ionian Sea. Our findings show that diagnostic XRF-CS ratios provide information on co-seismic depositional processes and sediment provenance. After integrating information on physical properties, particle size distribution, and geochemical composition, we conclude:

1. Pelagic deposits are identified by correlative peaks of Ca/Ti, Sr/Ti, and $CaCO_3$, $\delta^{13}C_{org} < -24‰$ VPDB, $C/N < 8$, by low HU and characteristic PCA plots, implying a background sediment consisting of biogenic constituents with lesser amounts of fine siliciclastic material.
2. STs contain detrital siliciclastic material derived from the continental margins, and commonly consists of a coarse basal stacked sand (STa), a homogenite (STb), a tsunamite/seiche laminite (STc), and a tsunamite backwash (STd) units. However, the sedimentary structures and composition of these units vary, depending on depositional setting (e.g., proximity to submarine canyons, isolated basin vs. open abyssal plain), varying sediment sources, energy of the triggering event and transport paths.
3. STa basal units are characterized by stacking of coarse sediments with variable composition. A source of terrigenous or coastal sediment is indicated by the increase of C/N, Zr/Ti, Ba/Ti, S/Ti, and decrease of $\delta^{13}C_{org}$. A high Sr/Ca ratio indicates sediment input with abundant aragonitic pteropod shell material from shelf and upper continental slope areas.

4. STb homogenite units, that are deposited during the waning flow of ST currents, are characterized by fining upward gran-size and enrichment of clay minerals with high Al.
5. STc and STd units consists of sediments of mixed marine and terrestrial sources with similar composition and structure in the different basins. Laminated STc units can be related to basin-wide seiching of the confined water mass. STd units include terrestrial sediment of tsunami wave erosion and backwash origin. The absence of the topmost reddish units (e.g., as in ST2/2), probably indicate that the triggering earthquake was not tsunamigenic.
6. C/N and $\delta^{13}C_{org}$ data from the different ST units in the three cores provide a powerful tool for identification of the sources and sedimentary processes.
7. A magnitude "threshold" of $\sim M_w = 6–7$ is required for generating slope failures, turbidity currents and the typical ST records in Ionian Sea confined basins that are not directly fed by a canyon system. Major earthquakes produce stacked turbidites while earthquakes less than Mw 6–7 only remobilize surficial slope sediments with marine indicator ratios (high Ca/Ti and Sr/Ti) similar to pelagic sediments.
8. ST2/2, which does not contain STc and STd units, is the only ST that was triggered by a non-tsunamigenic earthquake. Its basal part shows C/N always lower than 8 and falls in compositional range of marine or coastal sediment implying that tsunamigenic earthquakes are more efficient to deliver terrestrial C3 plants material to the deep ocean relative to non-tsunamigenic events.
9. The analysis of XRF-CS data from the Ionian Sea sediment shows that the elemental ratios were amenable to the statistical dimensional reduction. The first three principal components helped to identify four groups of variables that could explain the marine or terrestrial/coastal affinities. Ca/Ti, Sr/Ti, Zr/Rb, Fe/S, and Fe/Ca were selected as potential geochemical tracers to define the genetically different units in the ST beds and to correlate STs in separate basins. These proxies can be used also for preliminary ST characterization, in absence of other analytical data.
10. The interpretation of compositional features of the ST deposits allowed evaluating local effects related to the basin physiography and inferring sedimentary processes in different depositional settings to reconstruct source to sink processes and recognize geological characteristics of ST deposition, such as sediment provenance, sorting and diagenesis.

Data Availability Statement

All digital data used for this work will be available at ftp://ftp.ismar.cnr.it/outgoing/permanent_ro/GEOCHEM_SEISMO_TURBIDITES.

Acknowledgments
The authors thank the CALAMARE scientific party, Urania shipboard, and SOPROMAR parties for their contribution in core collection during the Urania cruises. The authors are grateful to C. Gelati and M. Imbriani, radiologists at Ospedale Maggiore in Bologna, for CAT scan acquisition. L. Langone and F. Savelli are acknowledged for OC analysis, S. Miserocchi for acquisition of XRF data at ISMAR (Institute of Marine Sciences), and T. Tesi for fruitful discussions. This work has benefited from funding provided by the CNR for the R/V Urania shiptime. ISMAR paper no. 2058. The authors acknowledge the Editor Whitney Behr, the Associate Editor Maria Giuditta Fellin, Witold Szczuciński and an anonymous reviewer for their suggestions and comments that have contributed to improve the original version of the manuscript.

References

Arai, K., Naruse, H., Miura, R., Kawamura, K., Hino, R., Ito, Y., et al. (2013). Tsunami-generated turbidity current of the 2011 Tohoku-Oki earthquake. *Geology*, *41*(11), 1195–1198. https://doi.org/10.1130/G34777.1

Bao, R., Strasser, M., McNichol, A. P., Haghipour, N., McIntyre, C., Wefer, G., & Eglinton, T. I. (2018). Tectonically-triggered sediment and carbon export to the Hadal zone. *Nature Communications*, *9*, 121. https://doi.org/10.1038/s41467-017-02504-1

Baratta, M. (1910). La catastrofe sismica calabro-messinese (28 Dicembre 1908). Relazione alla Società Geografica Italiana (Vol. 2, pp. XV, 426). *Roma, Presso la Società Geografica Italiana*. Retrieved from https://www.worldcat.org/title/terremoto-calabro-siculo-del-28-dicembre-1908-messina/oclc/38646170

Beck, C., Mercier de Lépinay, B., Schneider, J.-L., Cremer, M., Çağatay, N., Wendenbaum, E., et al. (2007). Late Quaternary co-seismic sedimentation in the Sea of Marmara's deep basins. In F. Bourrouilh-Le Jan, C. Beck, & D. Gorsline (Eds.), *Sedimentary Records of Catastrophic Events*. Sedimentary Geology Special Issues (Vol. 199, pp. 65–89). https://doi.org/10.1016/j.sedgeo.2005.12.031

Besse, P. (1992). PCA stability and choice of dimensionality. *Statistics & Probability Letters*, *13*, 405–410. https://doi.org/10.1016/0167-7152(92)90115-l

Billi, A., Funiciello, R., Minelli, L., Faccenna, C., Neri, G., Orecchio, B., & Presti, D. (2008). On the cause of the 1908 Messina tsunami, southern Italy. *Geophysics Research Letters*, *35*(6), L06301. https://doi.org/10.1029/2008GL033251

Boyle, E. A. (1983). Manganese carbonate overgrowths on foraminifera tests. *Geochimica et Cosmochimica Acta*, *47*, 1815–1819. https://doi.org/10.1016/0016-7037(83)90029-7

Bryant, F. B., & Yarnold, P. R. (1995). Principal-components analysis and exploratory and confirmatory factor analysis. In L. G. Grimm & P. R. Yarnold (Eds.), *Reading and understanding multivariate statistics* (pp. 99–136). American Psychological Association.

Buckley, D. E., & Cranston, R. E. (1988). Early diagenesis in deep sea turbidites: The imprint of paleo-oxidation zones. *Geochimica et Cosmochimica Acta*, *52*, 2925–2939.

Çağatay, M. N., Erel, L., Bellucci, L. G., Polonia, A., Gasperini, L., Eriş, K. K., et al. (2012). Sedimentary earthquake records in the İzmit Gulf, Sea of Marmara, Turkey. *Sedimentary Geology*, *282*, 347–359. https://doi.org/10.1016/j.sedgeo.2012.10.001

Chagué-Goff, C., Szczucinski, W., & Shinozaki, T. (2017). Applications of geochemistry in tsunami research: A review. *Earth-Science Reviews*, *165*, 203–244. https://doi.org/10.1016/j.earscirev.2016.12.003

Chaillou, G., Anschutz, P., Dubrulle, C., & Lecroart, P. (2007). Transient states in diagenesis following the deposition of a gravity layer: Dynamics of O_2, Mn, Fe and N-species in experimental units. *Aquatic Geochemistry*, *13*, 157–172. https://doi.org/10.1007/s10498-007-9013-0

Chapron, E., Beck, C., Pourchet, M., & Deconinck, J. F. (1999). 1822 earthquake-triggered homogenite in Lake Le Bourget (NW Alps). *Terra Nova*, *11*, 86–92. https://doi.org/10.1046/j.1365-3121.1999.00230.x

Chester, R. (2000) *Marine geochemistry* (2nd ed., p. 520). Unwin Hyman, Wiley-Blackwell. ISBN-I 3:978-94-010-9490-0. https://doi.org/10.1007/978-94-010-9488-7

Davis, J. C. (1986). *Statistics and data analysis in geology* (2nd ed., p. 646). John Wiley & Sons Inc.

De Lange, G. J. (1986). Early diagenetic reactions in interbedded pelagic and turbiditic sediments in the Nares Abyssal Plain (western North Atlantic): Consequences for the composition of sediment and interstitial water. *Geochimica et Cosmochimica Acta*, *50*(12), 2543–2561. https://doi.org/10.1016/0016-7037(86)90209-7

Gaetani, G. A., & Cohen, A. L. (2006). Element partitioning during precipitation of aragonite from seawater: A framework for understanding paleoproxies. *Geochimica et Cosmochimica Acta*, *70*, 4617–4634. https://doi.org/10.1016/j.gca.2006.07.008

Giuliani, S., Bellucci, L. G., Çağatay, M. N., Polonia, A., Piazza, R., Vecchiato, M., et al. (2017). The impact of the 1999 Mw 7.4 event in the İzmit Bay (Turkey) on anthropogenic contaminant (PCBs, PAHs and PBDEs) concentrations recorded in a deep sediment core. *The Science of the Total Environment*, *590–591*, 799–808. https://doi.org/10.1016/j.scitotenv.2017.03.051

Goff, J., Goto, K., Chagué, C., Watanabe, M., Gadd, P. S., & King, D. N. (2018). New Zealand's most easterly palaeotsunami deposit confirms evidence for major trans-Pacific event. *Marine Geology*, *404*, 158–173. https://doi.org/10.1016/j.margeo.2018.08.001

Goldfinger, C., Patton, J. R., Van Daele, M., Moernaut, J., Nelson, C. H., De Batist, M., et al. (2014). Can turbidites be used to reconstruct a paleo earthquake record for the central Sumatran margin?: COMMENT. *Geology Society of America*, *42*, e344. https://doi.org/10.1130/G35510C.110.1130/g35558c.1

Hammer, Ø., Harper, D. A. T., & Ryan, P. D. (2001). PAST: Paleontological statistics software package for education and data analysis. *Palaeontologia Electronica*, *4*(1), 1–9.

Hedges, J. I., & Stern, J. H. (1984). Carbon and nitrogen determinations of carbonate containing solids. *Limnology & Oceanography*, *29*, 657–663. https://doi.org/10.4319/lo.1984.29.3.0657

Heezen, B. C., & Ewing, M. (1952). Turbidity currents and submarine slumps, and the 1929 Grand Banks earthquake. *American Journal of Science*, *250*, 849–873. https://doi.org/10.2475/ajs.250.12.849

Jarvis, I., Moreton, J., & Gérard, M. (1998). Chemostratigraphy of Madeira Abyssal Plain Miocene-Pleistocene turbidites, Site 950. *Proceedings of the Ocean Drilling Program, Scientific Results*, *157*, 535–558.

Kastens, K. A. (1984). Earthquakes as a triggering mechanism for debris flows and turbidites on the Calabrian Ridge. *Marine Geology*, *55*, 13–33. https://doi.org/10.1016/0025-3227(84)90130-0

Kastens, K. A., & Cita, M. B. (1981). Tsunami-induced sediment transport in the abyssal Mediterranean Sea. *Geological Society of America Bulletin*, *92*, 845–857. https://doi.org/10.1130/0016-7606(1981)92<845:tstita>2.0.co;2

Keul, N., Peijnenburg, K. T. C. A., Andersen, N., Kitidis, V., Goetze, E., & Schneider, R. R. (2017). Pteropods are excellent recorders of surface temperature and carbonate ion concentration. *Nature Scientific Reports*, *7*, 12645. https://doi.org/10.1038/s41598-017-11708-w

Kioka, A., Schwestermann, T., Moernaut, J., Ikehara, K., Kanamatsu, T., McHugh, C. M., et al. (2019). Megathrust earthquake drives drastic organic carbon supply to the hadal trench. *Scientific Reports*, *9*, 1553. https://doi.org/10.1038/s41598-019-38834-x

Köng, E., Zaragosi, S., Schneider, J.-L., Garlan, T., Bachèlery, P., Sabine, M., & San Pedro, L. (2017). Gravity-driven deposits in an active margin (Ionian Sea) over the last 330,000 years. *Geochemistry, Geophysics, Geosystems*, *18* (11), 4186–4210. https://doi.org/10.1002/2017GC006950

Köng, E., Zaragosi, S., Schneider, J.-L., Garlan, T., Bachèlery, P., San Pedro, L., et al. (2016). Untangling the complex origin of turbidite activity on the Calabrian Arc (Ionian Sea) over the last 60 ka. *Marine Geology*, *373*, 11–25. https://doi.org/10.1016/j.margeo.2015.12.010

Lamb, A. L., Wilson, G. P., & Leng, M. J. (2006). A review of coastal palaeoclimate and relative sea-level reconstructions using $\delta^{13}C$ and C/N ratios in organic material. *Earth-Science Reviews*, *75*, 29–57. https://doi.org/10.1016/j.earscirev.2005.10.003

Lavallee, K. D., Kineke, G. C., & Milligan, T. G. (2019). Variability of cohesive particle characteristics in an energetic estuary: Flocs vs. aggregates. *Estuaries and Coasts*, *43*(25), 39–55. https://doi.org/10.1007/s12237-019-00655-6

McGarr, A. (1965). Excitation of seiches in channels by seismic waves. *Journal of Geophysical Research*, *70*(4), 847–854. https://doi.org/10.1029/JZ070i004p00847

McHugh, C. M., Kanamatsu, T., Seeber, L., Bopp, R., Cormier, M.-H., & Usami, K. (2016). Remobilization of surficial sediment triggered by the A.D. 2011 Mw9 Tohoku-Oki earthquake and tsunami along the Japan Trench. *Geology*, *44*(5). https://doi.org/10.1130/G37650

McHugh, C. M., Kanamatsu, T., Seeber, L., Bopp, R., Cormier, M.-H., Usami, K., et al. (2011). Offshore sedimentary effects of the 12 January 2010 Haiti earthquake. *Geology*, *39*(8), 723–726. https://doi.org/10.1130/G31815.1

McHugh, C. M., Seeber, L., Rasbury, T., Strasser, M., Kioka, A., Kanamatsu, T., et al. (2020). Isotopic and sedimentary signature of megathrust ruptures along the Japan subduction margin. *Marine Geology*, *428*, 106283. https://doi.org/10.1016/j.margeo.2020.106283

Pattiaratchi, C. B., & Wijeratne, E. M. S. (2009). Tide Gauge Observations of 2004–2007 Indian Ocean Tsunamis from Sri Lanka and Western Australia. *Pure and Applied Geophysics*, *166*, 233–258. https://doi.org/10.1007/s00024-008-0434-5

Polonia, A., Bonatti, E., Camerlenghi, A., Lucchi, R. G., Panieri, G., & Gasperini, L. (2013). Mediterranean megaturbidite triggered by the AD 365 Crete earthquake and tsunami. *Scientific Reports*, *3*, 1285. https://doi.org/10.1038/srep01285

Polonia, A., Nelson, C. H., Romano, S., Vaiani, S. C., Colizza, E., Gasparotto, G., & Gasperini, L. (2017). A depositional model for seismo-turbidites in confined basins based on Ionian Sea deposits. *Marine Geology*, *384*, 177–198. https://doi.org/10.1016/j.margeo.2016.05.010

Polonia, A., Panieri, G., Gasperini, L., Gasparotto, G., Bellucci, L. G., & Torelli, L. (2013). Turbidite paleoseismology in the Calabrian Arc subduction complex (Ionian Sea). *Geochemistry, Geophysics, Geosystems*, *14*, 112–140. https://doi.org/10.1029/2012GC004402

Polonia, A., Romano, S., Çağatay, N. M., Capotondi, L., Gasparotto, G., Gasperini, L., et al. (2015). Is repetitive slumping during sapropel S1 related to paleo-earthquakes? *Marine Geology*, *361*, 41–52. https://doi.org/10.1016/j.margeo.2015.01.001

Polonia, A., Torelli, L., Artoni, A., Carlini, M., Faccenna, C., Ferranti, L., et al. (2016). The Ionian and Alfeo-Etna fault zones: New segments of an evolving plate boundary in the central Mediterranean Sea? *Tectonophysics*, *675*, 69–90. https://doi.org/10.1016/j.tecto.2016.03.016

Polonia, A., Torelli, L., Gasperini, L., Cocchi, L., Muccini, F., Bonatti, E., et al. (2017). Lower plate serpentinite diapirism in the Calabrian Arc subduction complex. *Nature Communications*, *8*(1), 2172. https://doi.org/10.1038/s41467-017-02273-x

Polonia, A., Vaiani, C. S., & De Lange, G. (2016). Did the AD 365 Crete earthquake/tsunami trigger synchronous giant turbidity currents in the Mediterranean Sea? *Geology*, *44*, 191–194. https://doi.org/10.1130/G37486.1

Pongpiachan, S., & Schwarzer, K. (2013). A critical review and evaluation of applying semi-volatile organic compounds (SVOCs) as a geochemical tracer to indicate tsunami backwash. *Science of Tsunami Hazards*, *32*, 236–280.

R Core Team. (2020). *R: A language and environment for statistical computing*. R Foundation for Statistical Computing. Retrieved from http://www.R-project.org/

Rothwell, R. G., & Croudace, I. W. (2015). Twenty years of XRF core scanning marine sediments: What do geochemical proxies tell us? In I. W. Croudace (Ed.), *Chapter 2 in micro-XRF studies of sediment cores: A perspective on capability and application in the environmental sciences* (Vol. 17, pp. 25–102). Rothwell R.G. https://doi.org/10.1007/978-94-017-9849-5_1

Sakuna-Schwartz, D., Feldens, P., Schwarzer, K., Khokiattiwong, S., & Statteggee Stattegger, K. (2015). Internal structure of event layers preserved on the Andaman Sea continental shelf, Thailand: Tsunami vs. storm and flash-flood deposits. *Natural Hazard and Earth System Sciences*, *15*, 1181–1199. https://doi.org/10.5194/nhess-15-1181-2015

San Pedro, L., Babonnea, N., Gutschera, M.-A., & Cattaneo, A. (2017). Origin and chronology of the Augias deposit in the Ionian Sea (Central Mediterranean Sea), based on new regional sedimentological data. *Marine Geology*, *384*, 199–213. https://doi.org/10.1016/j.margeo.2016.05.005

Schwestermann, T., Huang, J., Konzett, J., Kioka, A., Wefer, G., Ikehara, K., et al. (2020). Multivariate statistical and multiproxy constraints on earthquake-triggered sediment remobilization processes in the central Japan Trench. *Geochemistry, Geophysics, Geosystems*, *21*, e2019GC008861. https://doi.org/10.1029/2019GC008861

Siesser, W. G., & Rogers, J. (1971). An investigation of the suitability of four methods used in routine carbonate analysis of marine sediments. *Deep Sea Research and Oceanographic Abstracts*, *18*(1), 135–139. https://doi.org/10.1016/0011-7471(71)90021-0

Stanley, D. J. (1981). Unifites: Structurless muds of gravity-flow origin in Mediterranean basins. *Geo-Marine Letters*, *1*(2), 77–83. https://doi.org/10.1007/bf02463322

Sumner, E. J., Siti, M. I., McNeill, L. C., Talling, P. J., Henstock, T. J., Wynn, R. B., et al. (2013). Can turbidites be used to reconstruct a paleoearthquake record for the central Sumatran margin? *Geology*, *41*(7), 763–766. https://doi.org/10.1130/g34298.1

Sun, C., Graff, M., & Liang, Y. (2017). Trace element partitioning between plagioclase and silicate melt: The importance of temperature and plagioclase composition, with implications for terrestrial and lunar magmatism. *Geochimica et Cosmochimica Acta*, *206*, 273–295. https://doi.org/10.1016/j.gca.2017.03.003

Szczuciński, W. (2020). Post-depositional changes to tsunami deposits and their preservation potential. In M. Engel, J. Pilarczyk, S. Matthias, M. D. Brill, & Ed Garrett (Eds.), *Geological records of tsunamis and other extreme waves*. Elsevier. https://doi.org/10.1016/B978-0-12-815686-5.00021-3

Thomson, J., Higgs, N. C., Croudace, I. W., Colley, S., & Hyde, D. J. (1993). Redox zonation of elements at an oxic/post-oxic boundary in deep-sea sediments. *Geochimica et Cosmochimica Acta*, *57*, 579–595. https://doi.org/10.1016/0016-7037(93)90369-8

Thomson, J., Higgs, N. C., Jarvis, I., Hyde, D. J., Colley, S., & Wilson, T. R. S. (1986). The behavior of manganese in Atlantic carbonate sediments. *Geochimica et Cosmochimica Acta*, *50*, 1807–1818. https://doi.org/10.1016/0016-7037(86)90140-7

Thomson, J., Jarvis, I., Green, D. R. H., & Green, D. (1998). Oxidation fronts in Madeira Abyssal Plain turbidites: Persistence of early diagenetic trace-element enrichments during burial, Site 950. *Proceedings of the Ocean Drilling Program, Scientific Results*, *157*. https://doi.org/10.2973/odp.proc.sr.157.130.1998

TIBCO Software Inc. (2018). *STATISTICA (data analysis software system), version 13*. TIBCO Software Inc.

Tipmanee, D., Deelaman, W., Pongpiachan, S., Schwarzer, K., & Sompongchaiyakul, P. (2012). Using Polycyclic Aromatic Hydrocarbons (PAHs) as a chemical proxy to indicate Tsunami 2004 backwash in Khao Lak coastal area, Thailand. *Natural Hazards and Earth System Sciences*, *12*, 1441–1451. https://doi.org/10.5194/nhess-12-1441-2012

Tripsanas, E. K., Bryant, W. R., & Phaneuf, B. A. (2004). Depositional processes of uniform mud deposits (unifites), Hedberg Basin, northwest Gulf of Mexico: New perspectives. In W. W. Sager, W. R. Bryant, E. H. Doyle, & prefacers (Eds.), High-resolution studies of continental margin geology and geohazards: AAPG Bulletin (Vol. 88/6, pp. 825–840). https://doi.org/10.1306/01260403104

Van Daele, M., Cnudde, V., Duyck, P., Pino, M., Urria, R., & De Batist, M. (2014). Multidirectional, synchronously-triggered seismo-turbidites and debrites revealed by X-ray computed tomography (CT). *Sedimentology*, *61*(4), 861–880. https://doi.org/10.1111/sed.12070

Van Os, B., Visser, H.-J., Middelburg, J. J., & De Lange, G. J. (1993). Occurrence of thin, metal-rich layers in deep-sea sediments: A geochemical characterization of copper mobilization. *Deep Sea Research Research Part I: Oceanographic Research Papers*, *40*(9), 1713–1730. https://doi.org/10.1016/0967-0637(93)90028-2

Wilson, T. R. S., Thomson, J., Colley, S., Hydes, D. J., Higgs, N. C., & Sørensen, J. (1985). Early organic diagenesis: The significance of progressive subsurface oxidation fronts in pelagic sediments. *Geochimica et Cosmochimica Acta*, *49*, 811–822. https://doi.org/10.1016/0016-7037(85)90174-7

Yakupoğlu, N., Uçarkuş, G., Eriş, K. K., Henry, P., & Çağatay, M. N. (2019). Sedimentological and geochemical evidence for seismoturbidite generation in the Kumburgaz Basin, Sea of Marmara: Implications for earthquake recurrence along the Central High Segment of the North Anatolian Fault. *Sedimentary Geology*, *380*, 31–44. https://doi.org/10.1016/j.sedgeo.2018.11.002

References From the Supporting Information

Fralik, P. W., & Kronberg, B. I. (1997). Geochemical discrimination of clastic sedimentary rock sources. *Sedimentary Geology*, *113*(1–2), 111–124.

Orians, K. J., Boyle, E. A., & Bruland, K. W. (1990). Dissolved titanium in the open ocean. *Nature*, *348*(6299), 322–325.

Piva, A., Asioli, A., Schneider, R. R., Trincardi, F., Andersen, N., Colmenero-Hidalgo, E., et al. (2008). Climatic cycles as expressed in sediments of the PROMESS1 borehole PRAD1-2, central Adriatic, for the last 370 ka: 1. Integrated stratigraphy. *Geochemistry, Geophysics, Geosystems*, *9*(1), Q01R01. https://doi.org/10.1029/2007GC001713